

บทบาทของไอน้ำในปฏิกิริยาออกซิเดชันของเอทิลีนที่เร่งโดยแสงบนไททาเนียมไดออกไซด์

ในวชิภาคก๊าซ



นางสาวสุรียพร ศักดิ์นภาวุฒิ

วิทยานิพนธ์นี้เป็นส่วนหนึ่งของการศึกษาตามหลักสูตรปริญญาวิทยาศาสตรมหาบัณฑิต

สาขาวิชาวิศวกรรมเคมี ภาควิชาวิศวกรรมเคมี


คณะวิศวกรรมศาสตร์ จุฬาลงกรณ์มหาวิทยาลัย

ปีการศึกษา 2548

ISBN 974-17-5055-2

ลิขสิทธิ์ของจุฬาลงกรณ์มหาวิทยาลัย

ROLE OF WATER VAPOR IN PHOTOCATALYTIC OXIDATION OF
ETHYLENE OVER TITANIUM DIOXIDE IN GAS PHASE



Miss Sureeporn Saknaphawuth

สถาบันวิทยบริการ
จุฬาลงกรณ์มหาวิทยาลัย

A Thesis Submitted in Partial Fulfillment of the Requirements
for the Degree of Master of Engineering Program in Chemical Engineering

Department of Chemical Engineering

Faculty of Engineering


Chulalongkorn University

Academic Year 2005

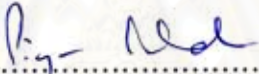
ISBN 974-17-5055-2


Thesis Title ROLE OF WATER VAPOR IN PHOTOCATALYTIC
 OXIDATION OF ETHYLENE OVER TITANIUM DIOXIDE
 IN GAS PHASE
By Miss Sureeporn Saknaphawuth
Field of Study Chemical Engineering
Thesis Advisor Akawat Sirisuk, Ph.D.

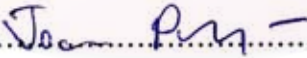
Accepted by the Faculty of Engineering, Chulalongkorn University in Partial
Fulfillment of the Requirements for the Master's Degree


.....Dean of the Faculty of Engineering
(Professor Direk Lavansiri, Ph.D.)

THESIS COMMITTEE


.....Chairman
(Professor Piyasan Praserttham , Dr.Ing.)


..... Thesis Advisor
(Akawat Sirisuk, Ph.D.)


..... Member
(Assistant Professor Joongjai Panpranot, Ph.D.)


.....Member
(Assistant Professor Seeroong Prichanont, Ph.D.)

สถาบันวิจัยปริชาน
จุฬาลงกรณ์มหาวิทยาลัย

สุรียพร ศักดิ์นภาวุฒิ: บทบาทของไอน้ำในปฏิกิริยาออกซิเดชันของเอทิลีนที่เร่งโดยแสงบนไททาเนียมไดออกไซด์ในวัฏภาคก๊าซ (ROLE OF WATER VAPOR IN PHOTOCATALYTIC OXIDATION OF ETHYLENE OVER TITANIUM DIOXIDE IN GAS PHASE) อ. ที่ปรึกษา: ดร.อัศวิต ศิริสุข, 89 หน้า, ISBN: 974-17-5055-2

เราทำการศึกษาปฏิกิริยาออกซิเดชันของเอทิลีนที่ใช้ตัวเร่งปฏิกิริยาแบบใช้แสงในเครื่องปฏิกรณ์แบบเบดนิ่งโดยใช้ไททาเนียมไดออกไซด์เป็นตัวเร่งปฏิกิริยาซึ่งเตรียมได้จากวิธีโซล-เจล เราทำการศึกษาผลของ อัตราการไหลของสารตั้งต้น ปริมาณความชื้น และอุณหภูมิในการทำปฏิกิริยา ที่มีผลต่อ จลนศาสตร์ของปฏิกิริยาออกซิเดชันที่ใช้ตัวเร่งปฏิกิริยาแบบใช้แสงของเอทิลีน เราใช้การวิเคราะห์ตามสมการการถดถอยแบบไม่เป็นเชิงเส้นในการฟิตข้อมูลทางจลนศาสตร์เข้ากับแบบจำลอง สมการของแลงเมียร์ฮินเชลวูดหอยเกินวัตสันสามารถอธิบายพฤติกรรมของปฏิกิริยาออกซิเดชันของเอทิลีนที่ใช้ตัวเร่งปฏิกิริยาแบบใช้แสงและให้การฟิตข้อมูลทางจลนศาสตร์ได้ดี ผลการศึกษาพบว่าอัตราการเกิดปฏิกิริยาของเอทิลีนลดลงเมื่อความชื้นสัมพัทธ์เพิ่มขึ้นแต่จะมีค่าเพิ่มขึ้นเมื่อเพิ่มอุณหภูมิในการทำปฏิกิริยา การดูดซับของน้ำบนพื้นผิวไททาเนียมสามารถแข่งขันกับการดูดซับของเอทิลีนบนพื้นผิว พลังงานกระตุ้นของปฏิกิริยา คือ 25.02 และ 6.78 กิโลจูลต่อโมล ที่ความชื้นสัมพัทธ์เท่ากับ 0 และ 100 เปอร์เซ็นต์ ตามลำดับ ค่าเอนทัลปีของการดูดซับของเอทิลีนคือ -11.3 และ 15.8 กิโลจูลต่อโมล ที่ความชื้นสัมพัทธ์เท่ากับ 0 และ 100 เปอร์เซ็นต์ ตามลำดับ

สถาบันวิทยบริการ

ภาควิชา.....วิศวกรรมเคมี..... ลายมือชื่อนิสิต... สุรียพร... ศักดิ์นภาวุฒิ

สาขาวิชา.....วิศวกรรมเคมี..... ลายมือชื่ออาจารย์ที่ปรึกษา.....

ปีการศึกษา..... 2548.....

##4670452121: MAJOR CHEMICAL ENGINEERING

KEY WORD: TITANIUM DIOXIDE / PHOTOCATALYTIC OXIDATION OF
ETHYLENE /NONLINEAR REGRESSION / RELATIVE HUMIDITY / LHHW
MODEL / ENTHALPY OF ADSORPTION/ TEMPERATURE/ VOCs

SUREEPORN SAKNAPHAWUTH: ROLE OF WATER VAPOR IN
PHOTOCATALYTIC OXIDATION OF ETHYLENE OVER TITANIUM
DIOXIDE IN GAS PHASE ADVISOR: AKAWAT SIRISUK, Ph.D. 89 pp.
ISBN 974-17-5055-2

The photocatalytic oxidation of ethylene was studied in a packed bed reactor using titanium dioxide that was prepared by a sol-gel method as a catalyst. Effects of several reaction parameters, namely, flow rate of reactant, humidity level, and temperature, on the kinetics of the photocatalytic oxidation process were investigated. Nonlinear regression analysis was employed to fit few proposed rate expression to the kinetic data. A Langmuir-Hinshelwood-Hougen-Watson rate expression was applied to describe the behavior of photocatalytic oxidation of ethylene and could give an adequate fitting to the kinetic data. The reaction rate of ethylene decreased with increasing relative humidity but increased with increasing reaction temperature. Water competes with ethylene for adsorption sites on titanium dioxide surface. The activation energies for the reaction were 25.02 and 6.78 kJ/mol at 0 and 100% relative humidity, respectively. The standard enthalpies of adsorption for ethylene were -11.3 and -15.8 kJ/mol at 0 and 100% relative humidity, respectively.

สถาบันวิทยบริการ
จุฬาลงกรณ์มหาวิทยาลัย

Department.....Chemical Engineering..... Student's signature..... Sureeporn Saknaphawuth
Field of study....Chemical Engineering..... Advisor's signature.....
Academic year...2005.....

ACKNOWLEDGEMENTS

This dissertation would not have been possible to complete without the support of the following individuals. Firstly, I would like to express my greatest gratitude to my advisor, Dr. Akawat Sirisuk, for his invaluable guidance during the course of this work, and I am also very grateful to Professor Dr. Piyasan Prasertdam, for his kind supervision over this thesis. Special thanks to Assistant Professor Joongjai Panpranot and Assistant Professor Seeroong Prichanont, members of the thesis committee for their kind cooperation.

The financial supports from the PTT Public Company Limited and Graduate School of Chulalongkorn University are also gratefully acknowledged.

Many thanks for kind suggestions and useful help to Mr. Watcharapong khaodee, Mr. Seubsakul Pokasem and many friends in the Research Center on Catalysis and Catalytic Reaction Engineering who always provide the encouragement and assistance along the thesis study.

Finally, I also would like to dedicate this thesis to my parents and my brother who have always been the source of my support and encouragement.

สถาบันวิทยบริการ
จุฬาลงกรณ์มหาวิทยาลัย

CONTENTS

	Page
ABSTRACT (IN THAI).....	iv
ABSTRACT (IN ENGLISH).....	v
ACKNOWLEDGEMENTS.....	vi
CONTENTS.....	vii
LIST OF TABLES.....	ix
LIST OF FIGURES.....	xi
CHAPTER	
I INTRODUCTION.....	1
II LITERATURE REVIEWS.....	2
2.1 Factors that can influence photocatalytic reactions.....	4
2.1.1 Effect of water vapor.....	4
2.1.2 Effect of temperature.....	7
2.1.3 Effect of flow rate.....	8
2.2 Kinetic models of photocatalytic oxidation.....	9
III THEORY.....	13
IV MATERIAL AND METHODS.....	17
4.1 Preparation of titanium dioxide.....	17
4.2 Characterization of catalysts.....	18
4.2.1 X-ray diffractometry (XRD).....	18
4.2.2 Nitrogen physisorption.....	18
4.3 Measurement of photocatalytic activity of catalysts.....	18
4.3.1 Material.....	18
4.3.2 Apparatus.....	19
4.3.2.1 Photoreactor.....	19
4.3.2.2 Gas Controlling System.....	20
4.3.3 Experimental procedure for determining the activity of the photocatalyst.....	20
V RESULTS AND DISCUSSION.....	23
5.1 Characterization of the catalysts.....	23
5.2 Kinetic modeling of the photocatalytic oxidation of ethylene.....	24
5.2.1 The design equation for the pack bed reactor.....	25

	Page
CHAPTER	
5.2.2 Statistical methods for analysis of kinetic data.....	28
5.2.3 Kinetic models for photocatalytic oxidation of ethylene.	29
5.2.4 Effect of water vapor on the photocatalytic oxidation of ethylene.....	30
5.2.4.1 Incorporation of concentration of water in the kinetic model.....	39
5.2.4.2 Results of nonlinear regression analyses.....	43
5.2.5 Effect of temperature on the photocatalytic oxidation of ethylene.....	49
VI CONCLUSIONS AND RECOMMENDATIONS FOR FUTURE RESEARCH.....	68
6.1 Conclusions.....	68
6.1.1 Characterization of titania.....	68
6.1.2 Kinetic studies of the photocatalytic oxidation of ethylene.....	68
6.2 Recommendations for future research.....	69
REFERENCES.....	70
APPENDICES.....	74
APPENDIX A: Calculation of the rate constant and the adsorption equilibrium constant.....	75
APPENDIX B: Calculation of the vapor pressure of water.....	82
APPENDIX C: Expression of the rate of reaction of ethylene.....	83
APPENDIX D: Classification of physical and chemical adsorption.....	87
VITA.....	89

LIST OF TABLES

TABLE	Page
4.1 Operating condition for gas chromatograph.....	22
5.1 Operating conditions for experimental set.....	29
5.2 Parameter estimates obtained from nonlinear regression analysis of kinetic data obtained at various relative humidities using a first-order LHHW rate expression. The temperature of the reaction is 90 °C.....	31
5.3 Enthalpy of formation and Gibbs free energy of formation at 25 °C, 1 atm.....	39
5.4 Parameter estimates obtained from nonlinear regression analysis of kinetic data using Model 1, 2, and 3. The temperature of the reaction is 90 °C.....	44
5.5 Mean residual sums of squares obtained from nonlinear regression analyses of kinetic data. The temperature of the reaction is 90 °C.....	45
5.6 Result of extra sum of squares test performed for Model 1 and Model 3..	46
5.7 Result of extra sum of squares test performed for Model 2 and Model 3..	46
5.8 Parameter estimates obtained from nonlinear regression analysis of kinetic data obtained at various temperatures based on a first-order LHHW rate expression. The relative humidity is 0 %.....	50
5.9 Parameter estimates obtained from nonlinear regression analysis of kinetic data obtained at various temperatures based on a first-order LHHW rate expression. The relative humidity is 100 %.....	50
5.10 Parameter estimates obtained from nonlinear regression analyses of an Arrhenius plot for rate constants at three temperatures (Figure 5.19a) and an Arrhenius-type plot for adsorption constants at three temperatures (Figure 5.19b). The relative humidity is 0 %. The intermediate temperature (T_0) is 76 °C.....	63
5.11 Parameter estimates obtained from nonlinear regression analyses of an Arrhenius plot for rate constants at three temperatures (Figure 5.20a) and an Arrhenius-type plot for adsorption constants at three temperatures (Figure 5.20b). The relative humidity is 100 %. The intermediate temperature (T_0) is 70 °C.....	64

TABLE	Page
5.12 Parameter estimates obtained from nonlinear regression analysis of a combined set of kinetic data obtained at three temperatures based on a first-order LHHW rate expression. The relative humidity is 0 %.....	65
5.13 Parameter estimates obtained from nonlinear regression analysis of a combined set of kinetic data obtained at three temperatures based on a first-order LHHW rate expression. The relative humidity is 100 %.....	65
A.1 Calculation of kinetic data in the form of $\frac{\ln(1 - X_A)}{X_A}$ and $\frac{W}{F_{A0} \cdot X_A}$. The reactions were performed at 90°C and 100% relative humidity.....	77
A.2 Calculation of data in the form of $\frac{X_A}{\ln(1 - X_A)}$ and $\frac{W}{F_{A0} \cdot \ln(1 - X_A)}$. The reactions were performed at 90°C and 100% relative humidity.....	79
A.3 Parameter estimates obtained from linear regression analyses of data for photocatalytic oxidation of ethylene at 90°C shown in Figures A.1 and A.2. The relative humidity is 100%.....	81
D.1 Typical Characteristics of Adsorption Processes.....	88

LIST OF FIGURES

FIGURE	Page
3.1 Promotion of an electron from the valence band to the conduction band on illumination of a semiconductor	13
3.2 Illustration of the major processes occurring on a semiconductor particle following electronic excitation.....	14
3.3 Surface and bulk electron trapping.....	15
4.1 Schematic representation of the photoreactor module. A side view of the reactor is shown at the left and an end view is on the right.....	19
4.2 Schematic diagram of the continuous flow reactor system.....	21
5.1 XRD patterns of titania calcined at 350 °C for 3 hours.....	24
5.2 Kinetic data for the photocatalytic oxidation of ethylene at 90 °C. The relative humidity is 0%. The line corresponds to the best fit curve determined from nonlinear regression analysis of the data in terms of first-order LHHW rate expression.....	32
5.3 Kinetic data for the photocatalytic oxidation of ethylene at 90 °C. The relative humidity is 20%. The line corresponds to the best fit curve determined from nonlinear regression analysis of the data in terms of first-order LHHW rate expression.....	33
5.4 Kinetic data for the photocatalytic oxidation of ethylene at 90 °C. The relative humidity is 40%. The line corresponds to the best fit curve determined from nonlinear regression analysis of the data in terms of first-order LHHW rate expression.....	34
5.5 Kinetic data for the photocatalytic oxidation of ethylene at 90 °C. The relative humidity is 60%. The line corresponds to the best fit curve determined from nonlinear regression analysis of the data in terms of first-order LHHW rate expression.....	35
5.6 Kinetic data for the photocatalytic oxidation of ethylene at 90 °C. The relative humidity is 80%. The line corresponds to the best fit curve determined from nonlinear regression analysis of the data in terms of first-order LHHW rate expression.....	36

FIGURE	Page
5.7 Kinetic data for the photocatalytic oxidation of ethylene at 90 °C. The relative humidity is 100%. The line corresponds to the best fit curve determined from nonlinear regression analysis of the data in terms of first-order LHHW rate expression.....	37
5.8 Kinetic data for the photocatalytic oxidation of ethylene at various relative humidities. The temperature of the reaction is 90 °C. The lines correspond to the best fit curves as determined from nonlinear regression analyse of the data using first-order LHHW rate expression...	38
5.9 Plot of the expected conversion of ethylene versus the conversion measured from the experiments for photocatalytic oxidation of ethylene. The line corresponding to $y = x$ is included as reference.....	47
5.10 Kinetic data for the photocatalytic oxidation of ethylene. The temperature is 90 °C. The open circles represent the kinetic data obtained from the experiments. The lines represent the expected conversion determined using nonlinear regression analysis of the data based on Model 1.....	48
5.11 Kinetic data for the photocatalytic oxidation of ethylene at 62 °C. The relative humidity is 0%. The line corresponds to the best fit curve determined from nonlinear regression analysis of the data based on a first-order LHHW rate expression.....	51
5.12 Kinetic data for the photocatalytic oxidation of ethylene at 76 °C. The relative humidity is 0%. The line corresponds to the best fit curve determined from nonlinear regression analysis of the data based on a first-order LHHW rate expression.....	52
5.13 Kinetic data for the photocatalytic oxidation of ethylene at 90 °C. The relative humidity is 0%. The line corresponds to the best fit curve determined from nonlinear regression analysis of the data based on a first-order LHHW rate expression.....	53

FIGURE	Page
5.14 Kinetic data for the photocatalytic oxidation of ethylene at various temperatures. The relative humidity is 0%. The lines correspond to the best fit curves determined from nonlinear regression analyse of the data based on a first-order LHHW rate expression.....	54
5.15 Kinetic data for the photocatalytic oxidation of ethylene at 50 °C. The relative humidity is 100%. The line corresponds to the best fit curve determined from nonlinear regression analysis of the data based on a first-order LHHW rate expression.....	55
5.16 Kinetic data for the photocatalytic oxidation of ethylene at 70 °C. The relative humidity is 100%. The line corresponds to the best fit curve determined from nonlinear regression analysis of the data based on a first-order LHHW rate expression.....	56
5.17 Kinetic data for the photocatalytic oxidation of ethylene at 90 °C. The relative humidity is 100%. The line corresponds to the best fit curve determined from nonlinear regression analysis of the data based on a first-order LHHW rate expression.....	57
5.18 Kinetic data for the photocatalytic oxidation of ethylene at three temperatures. The relative humidity is 0%. The lines correspond to the best fit curves determined from nonlinear regression analyse of the data based on a first-order LHHW rate expression.....	58
5.19 (a) Arrhenius plot for rate constants at three temperatures. (b) Arrhenius-type plot for adsorption equilibrium constants obtained at three temperatures. The relative humidity is 0%.....	61
5.20 (a) Arrhenius plot for rate constants at three temperatures. (b) Arrhenius-type plot for adsorption equilibrium constants obtained at three temperatures. The relative humidity is 100%.....	62
A.1 The plot of data for photocatalytic oxidation of ethylene at 90°C based on Table A.1. The relative humidity is 100%.....	78
A.2 The plot of data for photocatalytic oxidation of ethylene at 90°C based on Table A.2. The relative humidity is 100%.....	80

CHAPTER I

INTRODUCTION

Heterogeneous photocatalysis has been extensively investigated for destruction of various environmentally harmful organic compounds in gas or aqueous phase (Raillard *et al.*, 2005). Photocatalysis has an advantage over adsorption by activated carbon in that it can completely decompose organic compounds rather than transfer to another phase (Zhang and Liu, 2004). Owing to its low toxicity, high reactivity, and low cost, titanium dioxide (TiO₂) is a well-known semiconductor that has been widely used as the photocatalyst for decomposition of a number of volatile organic compounds (VOCs). Several variables that may influence VOCs degradation rates of VOCs have been studied. These variables may include concentrations of VOCs, humidity, light intensity, types and amounts of photocatalysts, reaction temperature, and even the reactor configurations. Among these variables, both humidity and reaction temperature may either promote or inhibit the rate of photocatalytic degradation (Wu *et al.*, 2005).

TiO₂ has an energy bandgap of 3.2 eV between the valence and conduction bands. Under UV illumination, electrons in the valence band can be excited to the conduction band and create highly reactive electron-hole pairs, which can participate in charge transfer reactions with contaminants adsorbed on catalyst surface. The final products of photocatalytic oxidation are usually carbon dioxide and water (Amama *et al.*, 2001; Wan-kuen *et al.*, 2002). TiO₂ nanoparticles can be prepared using various methods, including vapor decomposition, solvothermal method, hydrothermal method, and sol-gel method (Li *et al.*, 2003). Sol-gel processes are widely used to synthesize metal oxides with nanoscaled microstructures. This process provides excellent chemical homogeneity and possibility of deriving unique metastable structures at low reaction temperatures.

In this research we focus on the study of the photocatalytic degradation of ethylene in the gas phase. Ethylene was chosen as a reactant because it is structurally simple, has relatively high reactivity, and is the parent compound of more widespread

VOCs of environmental concern, e.g. trichloroethylene and tetrachloroethylene (Fu *et al.*, 1996). Moreover ethylene can be completely oxidized into carbon dioxide and water, without producing any major intermediates (Park *et al.*, 1999). Effects of several reaction parameters, namely, flow rate of reactant, humidity level, and temperature, on the kinetics of the photocatalytic oxidation process were investigated. The data were fitted by nonlinear regression analyses to propose rate expression. Kinetic models developed using the nonlinear regression analyses of the data can be employed to determine the optimal operating conditions for the photocatalytic system and the kinetic models of the photocatalytic oxidation are essential to the design of large-scale photocatalytic reactors.

The objectives of this research are as follows:

1. To study the effects of flow rate of reactants, relative humidity, and temperature on photocatalytic oxidation of ethylene over titanium dioxide prepared via sol-gel method.
2. To determine the best-fit kinetic model for photocatalytic oxidation of ethylene over titanium dioxide using nonlinear regression analyses.

This thesis is arranged as follows:

Chapter II presents literature reviews of previous works related to various topics involved in the research.

Chapter III discusses principles of photocatalytic process and explains the development of design equation for the packed bed reactor.

Chapter IV describes materials and methods employed in this research.

Chapter V describes kinetic studies of the photocatalytic oxidation of ethylene and presents the results of the nonlinear regression analyses of the kinetic data.

Chapter VI presents overall conclusions of this research and recommendations for future research.



สถาบันวิทยบริการ
จุฬาลงกรณ์มหาวิทยาลัย

CHAPTER II

LITERATURE REVIEWS

This chapter consists of two main sections. Section 2.1 discusses the influencing factors on photocatalytic reactions. The factors included humidity, temperature, and flow rate. Section 2.2 is a review of the kinetic model of photocatalytic oxidation.

2.1 Factors that can influence photocatalytic reactions

The reaction rate of photocatalytic oxidation can be influenced by such factors as humidity, light intensity, temperature, contaminant concentrations, flow rate and oxygen concentration. The effects of some factors on reaction rate are reviewed below.

2.1.1 Effect of water vapor

TiO₂ surface carries weakly or strongly bound molecular water and hydroxyl groups created by the dissociative chemisorption of water. In the absence of water vapor, the photocatalytic degradation of some chemical compounds (e.g., toluene and formaldehyde) is seriously retarded and the total mineralization to CO₂ does not occur. However, excessive water vapor on the catalyst surface will lead to the decrease of reaction rate because water molecule can occupy the active sites of the reactants on the surface (Zhao and Yang, 2003).

Wang and coworkers (1999) studied the photocatalytic decomposition of cis-dichloroethylene with titanium dioxide under irradiation of UV light with wavelength of 365 nm and concentration of water vapor in the range between 100-900 μM. When the humidity was less than 108.33 μM, the reaction rate increased with increasing moisture, but when the humidity was more than 108.33 μM, the reaction rate increased appreciably. The result was similar to the photocatalytic reactions of toluene and formaldehyde by Obee and Brown (1995). They reported that at lower humidity the reaction rate increased with increasing humidity up to a certain limit. Beyond the

limit, increased humidity slowed down the reaction rate. For higher reactant concentration and lower humidity, the factor controlling reaction rate was related to the supply of OH free radicals. Since a higher reactant concentration increased the consumption of OH radicals, increased humidity could provide more OH radicals to raise the reaction rate. For higher humidity, the lowering of reaction rate can be due to the following reasons: a) The formation of hydroxyl group in the hydrolysis of TiO₂ can lead to hydrogen bonding or covalent adsorption of DCE. The hydrogen atom in water molecule can also form hydrogen bonding with oxygen from the surface hydroxyl group on TiO₂ (Wang *et al.*, 1998). This could create competition for adsorption sites between DCE and water. With fixed concentration of DCE, more water content would gradually increase the adsorption for water molecules; b) With more accumulation of water molecules on TiO₂ surface, water can surround the adsorption sites and block the adsorption of DCE (Wang *et al.*, 1999); c) The excitation mechanism proposed by Gonzalez-Elipé and coworkers (1979) suggested that the excitation center (Ti⁺³- O⁻) must be formed first to catch the electron/hole pair. Then, the desorption of water molecules became a key trigger step to yield a coordination site for oxygen attachment to release hydroxyl free radicals. These radicals form peroxy free radicals (HO₂·) by protonation for subsequent reaction with DCE. Under lower humidity, there exists a balance of desorption among water molecules, consumption of free radicals, and adsorption of water molecules (Raupp and Junio, 1993). This balance could be upset under increased humidity.

Wang and coworkers (1998) investigate the effect of water vapor on photocatalytic degradation of trichloroethylene in gas phase over TiO₂ supported on glass bead. The result showed that the reaction rate of TCE was decreased with an increasing humidity for moisture in the range of 9.4-1222.2 μM. Similar results were reported by Wang and Hsieh (1997), who reported that the conversion of TCE decreased with increasing humidity, and the decomposition of this could be inhibited by excessive moisture. Anderson and coworkers (1993) found that their reaction rates were independent of water vapor concentration for mole fractions of water between 4.2×10^{-4} and 8.5×10^{-3} when operating at 23 °C and between 6×10^{-3} and 0.027 at 58 °C. The mole fraction of TCE employed was 3.4×10^{-4} at both temperatures. While Amama and coworkers (2004) reported that Degradation of TCE to CO₂ increased from 52% at 0% relative humidity (RH) to 71% at 100% RH during the

heterogeneous photocatalytic degradation reaction but during the heterogeneous photochemical oxidation reaction it decreased from 27% at 0% relative humidity (RH) to 2% at 100% RH. The optimum RH for the heterogeneous photocatalytic degradation reaction is ~25% RH because both relatively high degradation of TCE to CO₂ and high reactivity of the heterogeneous photocatalytic degradation reaction can be achieved simultaneously. Yamazaki and coworkers (2001) observed the photocatalytic degradation of gaseous tetrachloroethylene on porous TiO₂ pellets. They reported that water vapor competed for the same adsorption sites on the TiO₂ surface. Therefore, reaction rates decreased when the mole fraction of H₂O was 50-60 times higher than that of photocatalytic degradation of tetrachloroethylene.

Raillard and coworkers (2004) investigated the effects of two different levels of relative humidity on the photocatalytic oxidation of acetone and 2-butanone over TiO₂-containing paper at a fixed temperature. The water vapor greatly inhibits photocatalytic oxidation of acetone for initial acetone concentrations ranging from 0 to 6 gm⁻³, but the water vapor has little effect on photocatalytic degradation of 2-butanone. Moreover, Peral and Ollis (1992) found that water vapor feed concentrations of 250 - 10000 mg m⁻³ in the feed inhibited acetone photooxidation of reactant but had no influence on the reaction rate of 1-butanol. These results may be explained in terms of competitive adsorption effects. Acetone is less strongly adsorbed on the surface of TiO₂ than 1-butanol. Consequently, water can displace acetone adsorbed on the surface of TiO₂ but cannot displace 1-butanol. Hence water inhibits the photocatalytic oxidation of acetone but not that of 1-butanol.

Luo and Ollis (1996) studied the influence of water vapor on toluene and found the influence of water on photocatalytic oxidation depended upon the characteristics of contaminants. Toluene oxidation rate increased by water concentration up to about 1650 ppmv at toluene concentration of 0-800 ppmv but began to decrease when water concentration increased to more than 4000 ppmv, and toluene degradation was inhibited at 6000 ppmv water concentration while Obee and Brown (1995) reported that the effect of water vapor concentration on the oxidation rate of formaldehyde was similar to toluene. The formaldehyde oxidation rate was enhanced to a highest point then decreased with the increase of water vapor concentration. The effect of humidity on the oxidation rate for different formaldehyde

levels showed that the influence of humidity was biggest when inlet formaldehyde concentration reached to 6.1 ppmv. When the relevant humidity range was roughly 15-60% relative humidity or 4000-16000 ppmv, the Langmuir-Hinghelwood correlation indicated that the formaldehyde oxidation rate was first-order for formaldehyde level below 10 ppmv.

2.1.2 Effect of temperature

Wu and coworkers (2005) employed TiO₂ photocatalyst to oxidize benzene in the gas phase at a temperature ranging from 100 to 200 °C and found that the reaction rate of benzene peaked at a reaction temperature of roughly 160-180 °C. Similar results were reported by Falconer and Magrini-Bair (1998), who reported that the photocatalytic reaction rate of acetaldehyde reached a peak at around 140 °C. According to the gas-solid catalysis theory, surface reaction includes three steps: reactant adsorption, chemical reaction, and product desorption. Increasing the reaction temperature not only increases the chemical reaction rate and product desorption rate, but also reduces the reactant adsorption rate (Fogler, 1999). The increase in chemical reaction rate and product desorption rate lead to the increase of reaction rate. In contrary, the decrease of reactant adsorption rate decreases the reaction rate. The slowest step is the rate-limiting step. In this work, the benzene reaction rate increased with increasing temperature, suggesting that the decrease in reactant adsorption rate did not affect the overall reaction. Therefore, the chemical reaction or product desorption was the slowest step in the reaction as they increased with temperature. Consequently, chemical reaction or product desorption was the rate-limiting step of photocatalytic reaction below 160–180 °C. With the chemical reaction rate or the product desorption rate increasing continuously and the reactant adsorption rate decreasing with increasing temperature, the chemical reaction rate or the product desorption rate gradually exceeded the reactant adsorption rate, which gradually became the slowest rate step. Thus, the rate limiting step shifted from the chemical reaction or the product desorption to the reactant adsorption (Wu *et al.*, 2005). Moreover, Yamazaki and coworkers (1999) found that the rate of photocatalytic oxidation of ethylene reached a plateau when the temperature was increased from 66 °C to 81.3 °C.

Yamazaki and coworkers (2001) used porous TiO₂ pellets to oxidize tetrachloroethylene in the gas phase. The reaction rate did not depend on temperature over the range of 43.9-77.6 °C, although the rate at 29.5 °C was smaller and that at 90.6 °C larger. Hager and coworkers (2000) reported that lower conversion of trichloroethylene and tetrachloroethylene was obtained when temperature was increased from 20 °C to 70 °C. Fu and coworkers (1996) studied the effect of temperature on the photocatalytic oxidation of ethylene over TiO₂ and platinumized TiO₂. They performed at two different feed concentration of water vapor and at temperatures from 30 °C to 100 °C. The result indicated that the rate of photocatalytic oxidation of ethylene increased with increasing temperature at both concentrations of water vapor and no appreciable oxidation of ethylene over the pure TiO₂ catalyst was observed under dark condition in this temperature range. The enhancement of the rate of oxidation of ethylene with increasing temperature may be due to a decreasing desorption of water when the temperature increases. For Pt/TiO₂ catalyst, not only increases the oxidation rate of ethylene but also increases the conventional heterogeneous catalytic reaction. In the dark reaction, the heterogeneous catalytic oxidation of ethylene occurred on the Pt/TiO₂ catalyst at temperature above 40 °C.

2.1.3 Effect of flow rate

Zhang and Liu (2004) studied the effect of flow rate on the decomposition of hexane at operating flow rates between 5 and 17 l/min. The reaction rate of hexane initially increased with flow rate and reached a plateau when the flow rate was larger than 12 l/min. Similar results were reported by Wang and coworker (1998) who investigated the photocatalytic oxidation of trichloroethylene (TCE) in gas phase. With flow rate of TCE in the range of 100-500 ml/min, the reaction rate increased with an increasing flow rate up to 300 ml/min, while at flow rate higher than 300 ml/min the rate was not affected. In heterogeneous catalysis, the possible rate-controlling steps are mass transfer and surface reaction steps. The reaction at low flow rate was under the influence of mass transfer, for which the increase in flow rate would increase the reaction rate, the mass transfer effect from the bulk phase to the surface decrease with increasing flow rate, and then, the reaction rate gradually levels off. When the flow rate was larger than 300 ml/min, the reaction rate was no longer

influenced by flow rate as a result of surface reaction control but not due to mass transfer effect.

Wang and Hsieh (1997) employed titanium dioxide to investigate photocatalytic degradation of trichloroethylene. They reported that for the flow rate of feed gas between 100-900 ml/min, the conversion decreased with an increasing flow rate. The decomposition of TCE at 900 ml/min was only 2.22%, indicating feed gas rapidly passing through the catalyst layer without a reaction.

2.2 Kinetic models of photocatalytic oxidation

The kinetic experiments are performed to study the photodegradation of objective compounds. The dependence of the degradation rate on the influencing factor (e.g. water vapor content, temperature, light intensity) are investigate and gotten from the corresponding kinetic data (Zhao and Yang , 2003).

Wu and coworkers (2005) studied the photocatalytic degradation of benzene vapor over titanium dioxide. They applied a bimolecular Langmuir – Hinshelwood (L-H) model to describe the competition adsorption reaction among benzene and water. Several assumption were made: (1) benzene and water are adsorbed on separate sites and without dissociation; (2) benzene and water react with each other; (3) reaction products, carbon dioxide, carbon monoxide and intermediates do not influence the observed oxidation rate, and the influence of any intermediates was neglected.

$$r_B = k_{LH} \frac{K_B C_B K_W C_W}{(1 + K_B C_B + K_W C_W)^2} \quad (2.1)$$

where k_{LH} denote the rate constant; K_B and K_W represent the Langmuir adsorption equilibrium constants of benzene and water vapor, respectively, and C_B and C_W are the gas-phase concentration of benzene and water vapor, respectively.

Wang and coworkers (1998) have examined the influence of water vapor on gas phase of trichloroethylene over TiO_2 supported on glass bead. The Langmuir-

Hinshelwood bimolecular from of the kinetic expressions was used in this investigation and the rate law is represented by the following equation:

$$r = k \left(\frac{K_1 C_r}{1 + K_1 C_r + K_2 C_w} \right) \left(\frac{K_4 C_w}{1 + K_3 C_r + K_4 C_w} \right) \quad (2.2)$$

where k is the rate constant; K_1 , K_2 , K_3 and K_4 the Langmuir adsorption equilibrium constants and C_r and C_w are the gas-phase concentration of trichloroethylene and water vapor, respectively. This model describes that the two ratio terms represent the competitive adsorption between TCE and water vapor for the same site, resulted in the most adequate fitting to their experiment results, and they found that the adsorption constant for TCE (K_3) of the second ratio term in this model is negative because the adsorption of water vapor molecules may lead to the desorption of TCE in the ratio term for water vapor molecule, i.e., the attraction of water vapor to the surface of TiO_2 is stronger than TCE, and replace original TCE at surface sites. Moreover, there has a probable cause which is the accumulation of intermediates at the surface of TiO_2 . Demeestere and coworkers (2004) reported that a trimolecular Langmuir-Hinshelwood model, including competitive adsorption TCE, its intermediates and CO_2 , could not fit the results adequately for the photocatalytic degradation of trichloroethylene in gas phase.

Zang and Lui (2004) used Langmuir-Hinshelwood model to describe of the hexane degradation by TiO_2/UV . When the water vapor or oxygen also varied, L-H model was found to provide a good correlation to the photocatalytic reaction rate data. The reaction rate is given by

$$r = k \left(\frac{K_1 C_h}{1 + K_1 C_h + K_2 C_w} \right) \left(\frac{K_4 C_w}{1 + K_3 C_h + K_4 C_w} \right) \quad (2.3)$$

The model represents adsorption of hexane and water on different types of sites with competitive adsorption, however water adsorbed on reaction sites of hexane does not involve the reaction, and hexane adsorbed on reaction sites of water does not involve the reaction either. And the reaction rate expression was used to correlate the experimental data in the $\text{O}_3/\text{TiO}_2/\text{UV}$ process:

$$r = k \left(\frac{K_1 C_h}{1 + K_1 C_h + K_2 C_w} \right) \left(\frac{K_4 C_w}{1 + K_3 C_h + K_4 C_w} \right) + k' C_o \quad (2.4)$$

where k is the surface rate constant; k' is the gas phase reaction rate constant; K_1, K_2 are the adsorption constant of contaminant such as hexane; K_3, K_4 the adsorption constant of water; and C_h, C_o and C_w are concentration of hexane, oxygen and water vapor, respectively. Because the O_3 /TiO₂/UV process the hydroxyl radical was generated via two pathways: (1) TiO₂ photocatalysis (TiO₂/UV) and (2) ozone photolysis (O₃/UV). Thus the degradation of hexane not only happens on the surface of photocatalyst but also occurs in the bulk of gas phase. The surface reaction on photocatalyst can be described with L-H model, and the reaction in the bulk phase can be described by first-order kinetics with ozone concentration if the hexane concentration is excessive.

Wang and coworkers (1999) investigated the photocatalytic degradation kinetics for dichloroethylene in vapor phase. The reaction rate can be postulated by the Langmuir-Hinshelwood bimolecular model. Surface adsorption of DCE on TiO₂ took place with competition of adsorption site between DCE and water molecule but not with oxygen molecule. Hence, the rate expression as following:

$$r = \frac{k K_{DCE} C_{DCE} K_{O_2} C_{O_2}}{(1 + K_{DCE} C_{DCE} + K_W C_W)(1 + K_{O_2} C_{O_2})} \quad (2.5)$$

Devahasdin and coworkers (2003) used TiO₂ photocatalyst to oxidize nitric oxide. The process involves a series of oxidation steps by the OH• radical: $NO \rightarrow HNO_2 \rightarrow NO_2 \rightarrow HNO_3$ and the intermediate species, HNO_2 , can be oxidized to NO_2 and H_2O . The former is then oxidized to HNO_3 , the major product deposited on the catalyst. The effects of space time and inlet concentration can be described with the L-H model that is shown below:

$$-r_{NO} = \frac{K'_A C_{NO} C_{H_2O} - K'_B C_{NO_2}}{(1 + K'_{H_2O} C_{H_2O} + K'_{NO} C_{NO} + K'_{NO_2} C_{NO_2})^2} \quad (2.6)$$

where $-r_{NO}$ denotes the disappearance rate of NO; K'_A , K'_B are the reaction rate constants; K'_{H_2O} , K'_{NO} , K'_{NO_2} are the adsorption equilibrium constant; and C_{NO} , C_{NO_2} , C_{H_2O} are the concentration of nitric oxide, nitrogen dioxide, and water in gas phase, respectively.



สถาบันวิทยบริการ
จุฬาลงกรณ์มหาวิทยาลัย

CHAPTER III

THEORY

This chapter describes the fundamental phenomena that occur in photocatalytic process.

Theory of photocatalytic oxidation

Semiconductor particles may be photoexcited to form electron donor sites (reducing sites) and electron acceptor sites (oxidizing sites), providing great scope as redox reagents.

The molecular orbitals of semiconductors have a band structure. The bands of interest in photocatalysis are the occupied valence band and the unoccupied conduction band. They are separated by energy distance referred to as the band gap (E_g). When the semiconductor is illuminated with the light of greater energy than that of the band gap, an electron is promoted from the valence band to the conduction band (Robertson, 1996). This process leaves a positive hole in the valence band as illustrated in Figure 3.1.

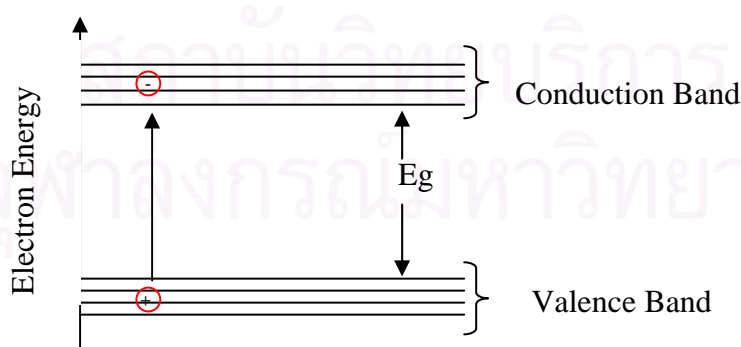


Figure 3.1 Promotion of an electron from the valence band to the conduction band on illumination of a semiconductor (Robertson, 1996).

The explanation of the phenomena occurring during the irradiation of semiconductor is summarized in Figure 3.2. When the semiconductor (SC) is illuminated with light of energy higher than or equal to the band gap energy (in step 1), an electron (e^-) in the valance band (VB) is excited to the conduction band (CB) with simultaneous generation of a hole (h^+) in the valance band. The excited electron (e^-_{CB}) and generation hole (h^+_{VB}) can move to the surface of semiconductor. The recombination of the electron and hole can be occurred on the surface or the bulk of the particle in a few nanoseconds to produce heat and light emission (in step 2). At the surface, photogenerated electrons (e^-_{CB}) can reduce an electron acceptor (A, an oxidant) in step 3 and photogenerated holes (h^+_{VB}) can oxidize an electron donor (D, a reductant) in step 4 (Tawkaew, 2003).

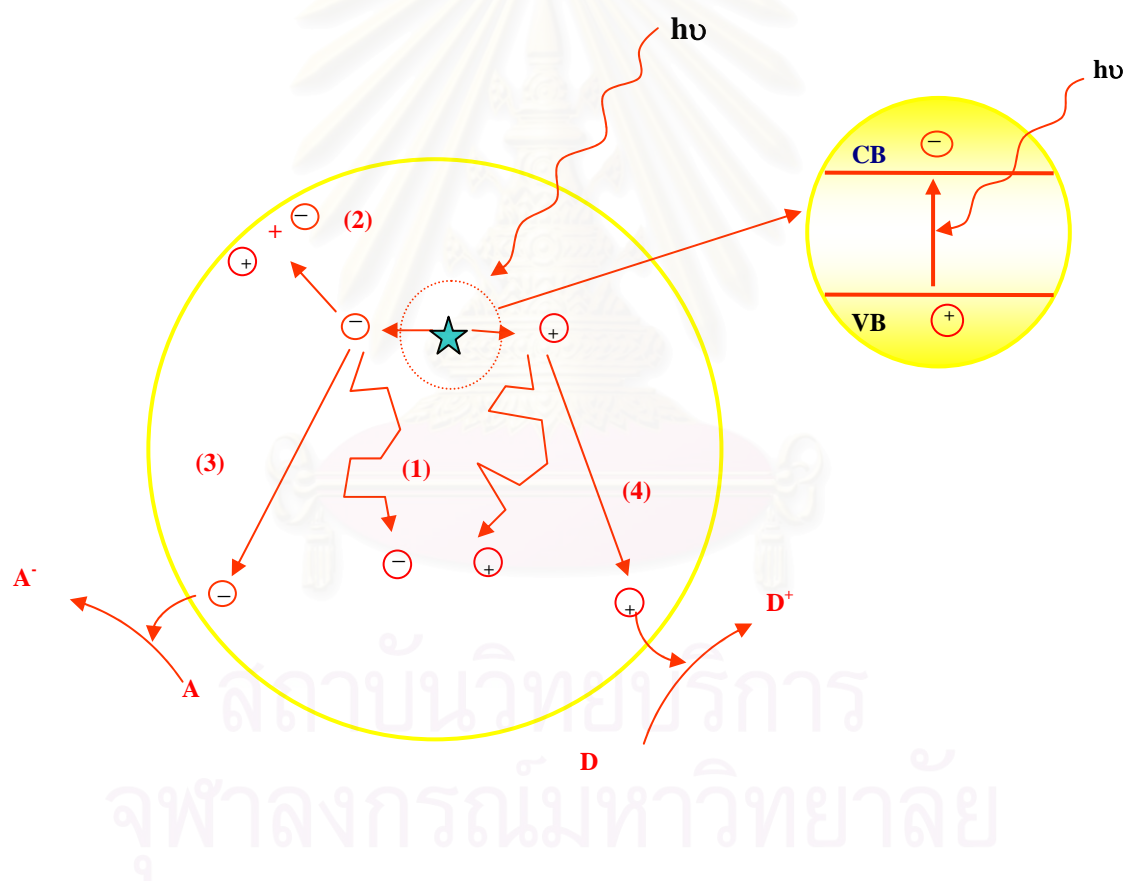


Figure 3.2 Illustration of the major processes occurring on a semiconductor particle following electronic excitation (Linsebigler *et al.*, 1995)

Light Absorption	$SC + h\nu \rightarrow e_{CB}^- + h_{VB}^+$	step 1
Recombination	$e_{CB}^- + h_{VB}^+ \rightarrow \text{heat or light}$	step 2
Reduction reaction	$A + e_{CB}^- \rightarrow A^-$	step 3
Oxidation reaction	$D + h_{VB}^+ \rightarrow D^+$	step 4

In Figure 3.3, the energy levels of the bulk and surface traps fall within the band gap. The surface and bulk traps are localized, and the electrons trapped in such states are thus associated with a particular site on the surface or in the bulk of the solid. The population of bulk and surface traps depend on two factors, namely, the decrease in entropy that occur when electrons are trapped, and the difference in relative energy between the traps and the bottom of the conduction band.

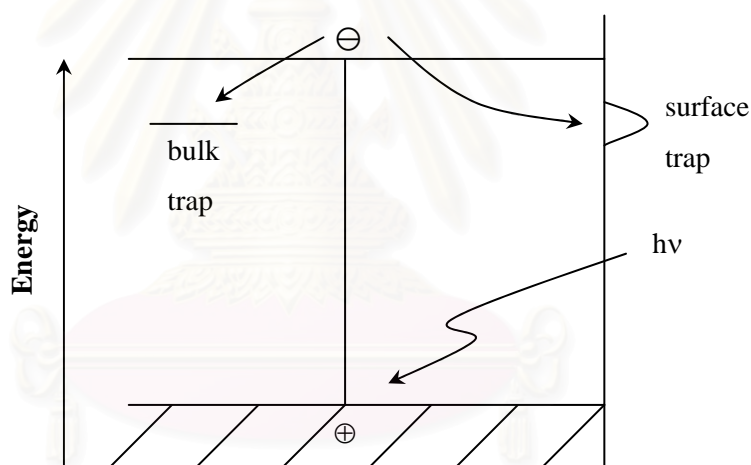


Figure 3.3 Surface and bulk electron trapping (Linsebigler *et al.*, 1995).

In aqueous solution, hydroxyl radicals ($\cdot\text{OH}$) production is favorable because of the abundance of hydroxyl groups and water molecules on the surface of catalyst. However, in the gas phase, organic substrates can themselves act as adsorbed traps for the photogenerated hole since in the gas phase, water molecules are not the predominant species in contact with the catalyst. Although in the presence of water vapor, OH groups are presented on the catalyst surface and their contribution to photooxidation can not be discarded (Alherici *et al.*, 1997).

When adsorbed water molecules are oxidized by holes, hydroxyl radicals, which have strong oxidizing power, are formed (Equations 3.1 and 3.2).



The hydroxyl radicals can then react with organic components, initially producing free radicals. When molecular oxygen is present (reactions always occur in the presence of oxygen from the air in the use of the photocatalyst for environment), it can react with these free radicals, produce organic peroxy radicals. These radicals can then take part in chain reactions. In a short time, organic compounds are completely degraded, i.e., converted into carbon dioxide and water.

Meanwhile, the electrons that are produced in the electron-hole pairs are also put to work. These electrons are used to reduce (i.e., add electrons) to oxygen in air. Because oxygen is easier to reduce than water, it will tend to be reduced, producing the superoxide radical anion (O_2^-).



The superoxide anion attaches itself to the peroxy radicals mentioned above. The resulting unstable product now contains at least four oxygens and can decompose to produce a carbon dioxide molecule. On the molecular scale, superoxide acts like a "supercharge", greatly increasing the oxidation process, which is in fact a form of combustion. In addition to this mechanism, another interpretation proposed recently is that the formation of atomic oxygen (O^\bullet), which is extremely reactive in air, leads to a direct attack on the carbon bonds in organic material.

CHAPTER IV

MATERIALS AND METHODS

This chapter describes the methods employed in the experimental work. Section 4.1 describes preparation of titanium dioxide to be used as photocatalysts, while section 4.2 discusses several characterization techniques for catalysts, including of X-ray diffractometry and nitrogen adsorption. Finally, the experimental apparatus and procedures used in evaluating the performance of the photocatalysts are explained in Section 4.3.

4.1 Preparation of titanium dioxide

Titanium dioxide was prepared using a sol-gel method, and titanium isopropoxide (Aldrich Chemical, Milwaukee, WI) was employed as a precursor. First, 7.33 ml of 70% nitric acid (Asia Pacific Specialty Chemicals Limited) was added to 1000 ml of distilled water. While the acidic solution was stirred, 83.5 ml of titanium isopropoxide was added slowly. The suspensions were stirred continuously at room temperature for about 3-4 days until clear sol was obtained. After that, the sol was dialyzed in a cellulose membrane with a molecular weight cutoff of 3500 (Spectrum Companies, Gardena, CA). Prior to use, the dialysis tubing was washed in an aqueous solution of 0.001M EDTA and 2% sodium hydrogen carbonate. The wash solution was prepared by dissolving 0.372 grams of EDTA (Asia Pacific Specialty Chemicals Limited) and 43 grams of sodium hydrogen carbonate powder, 99.93% (Fisher Scientific Chemical) in one liter of distilled water. Dialysis tubing was cut into sections of 32 cm in length and was submerged in the wash solution. Then the membrane was heated to 80 °C and held there for 30 minutes while simultaneously being stirred. After the solution was cooled to room temperature, the tubing was again washed with distilled water. The tubing was again immersed in one liter of fresh distilled water while being stirred continuously, and was heated to 80°C. The tubing was rinsed one more time and was stored in distilled water at 4°C until needed. The clear sol was placed in dialysis tubing. Then the tubing containing the sol was submerged in distilled water using a ratio of 100 ml of sol per 700 ml of distilled

water. The water was changed daily for 3-4 days until the pH of the water reached 3.5. To remove solvents, the dialyzed sol was left in ambient atmosphere overnight and was dried at 110°C. The resulting gel was then ground. Finally, titania nanoparticles were fired at temperature 350°C for the duration of 3 hours.

4.2 Characterization of catalysts

In order to determine properties of catalysts, various characterization techniques were employed. Such techniques are discussed in this section.

4.2.1 X-ray diffractometry (XRD)

XRD was employed to identify crystal phase, and crystallite size of metal oxide. The equipment used was a SIEMENS D 5000 X-ray diffractometer with CuK_α radiation with Ni filter in the 2θ range of 20-80° with a resolution of 0.04°.

4.2.2 Nitrogen physisorption

Nitrogen physisorption single point was determined at liquid nitrogen temperature of 77K. Brunauer-Emmett-Teller (BET) approach was utilized to determine specific surface area. The equipment used was a Micromeritics ChemiSorb 2750.

4.3 Measurement of photocatalytic activity of catalysts

The apparatus and experimental procedures employed to evaluate the performance of various photocatalysts were described in this section.

4.3.1 Material

The reactant gas used for this study was ethylene in air as supplied by Thai Industrial Gas Limited. The gas mixture contained 0.1 vol % ethylene in balance air.

4.3.2 Apparatus

Photoreactor system consists of a photoreactor and a gas controlling system.

4.3.2.1 Photoreactor

The photoreactor (see Figure 4.1) had two main components: an ultraviolet light source and the tubular packed bed reactor. The reactor was made from a Pyrex glass tube with a diameter of 5 mm and a length of 27 cm. The stainless steel tube is 1.5" in length and 3/8" in diameter connected to the both ends of the reactor. Two sampling points were located on the left and right of catalyst bed. The catalyst was packed between two quartz wool layers.

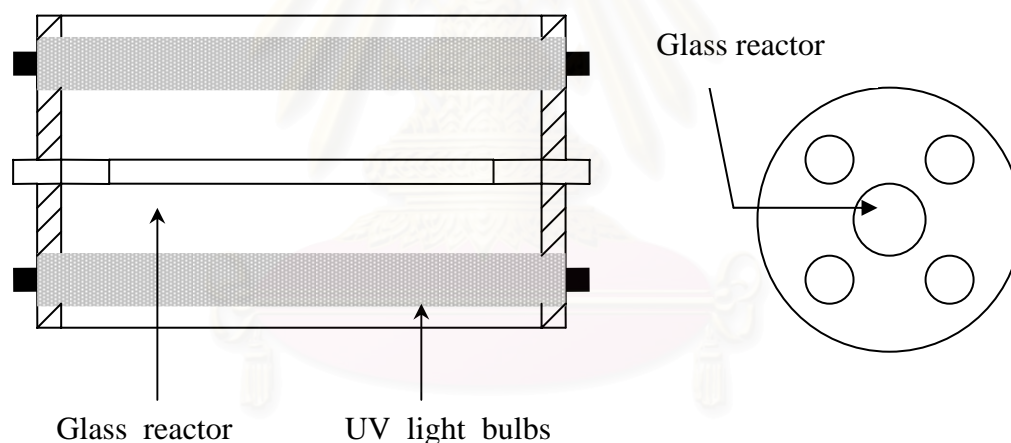


Figure 4.1 Schematic representation of the photoreactor module. A side view of the reactor is shown at the left and an end view is on the right.

Ultraviolet light sources were four blacklight blue fluorescent bulbs (8 Watts). Four light bulbs were located 1.5 cm away from the reactor in square configuration. The photoreactor was covered with two layers of aluminum foil to minimize radiation losses from the system.

4.3.2.2 Gas Controlling System

Each feed line reactant was equipped with a pressure gauge and a ball valve. Flow rate of gas was adjusted using mass flow controllers and was measured using a bubble flow meter.

4.3.3 Experimental procedure for determining the activity of the photocatalyst

The photocatalytic activity measurements were performed over 0.4 g of catalyst, which was packed in the reactor. The photoreactor was incorporated into the reactor system. Prior to each experiment, the reactor was supplied with air at a flow rate of 15 ml/min. The photocatalyst was illuminated by ultraviolet light sources for one hour in order to remove any organic compounds that might remain on the catalyst surface from previous experiments. Cooling air is fed to the side of the photoreactor to adjust the temperature to the desired level. The temperature of the reactor is monitored, using a K-type thermocouple, during this period to ascertain that the desired temperature is achieved in the photoreactor before starting an experiment.

After one hour, the setting of each controller was adjusted to obtain the desired flow rate of the feed. If a humid gas stream is needed for a particular experiment, a portion of the reactant gas was passed through a water saturator that served to saturate this gas with water. The humid stream was then recombined with the dry stream and combined stream entered the photoreactor. The flow rate of each gas was measured using a bubble flow meter. The diagram of the flow reactor system used to test the photocatalysts was shown in Figure 4.2.

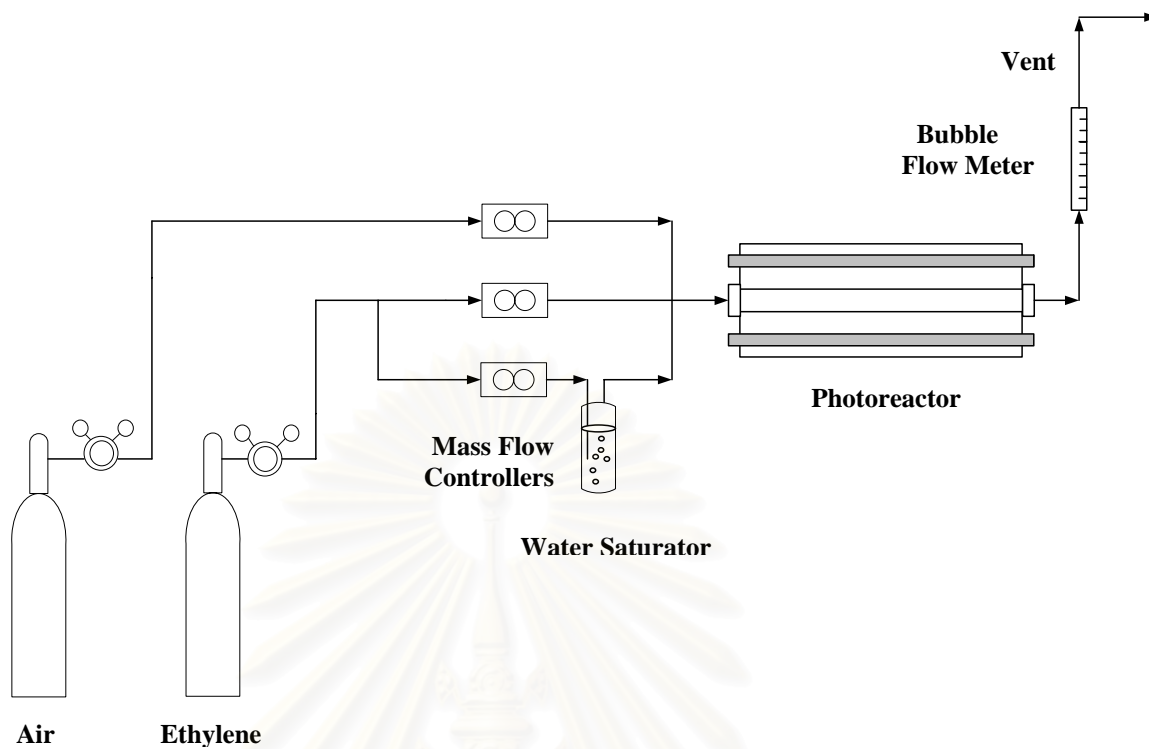


Figure 4.2 Schematic diagram of the continuous flow reactor system.

The effluent gas was sampled to determine the concentration of ethylene using GC-14B gas chromatograph (Shimadzu), equipped with a flame ionization detector. The operating conditions for the instrument were listed in Table 4.1. The concentration was measured every 20 minutes until steady state was achieved (as indicated by constant peak areas in the gas chromatograms).

สถาบันวิทยบริการ
จุฬาลงกรณ์มหาวิทยาลัย

Table 4.1 Operating conditions for gas chromatography

Gas Chromatograph	SHIMADZU GC-14B
Detector	FID
Column	VZ10
Carrier gas	H ₂ (99.999%)
Carrier gas flow (ml/min)	30 cc/min
Column temperature	
- initial (°C)	70
- final (°C)	70
Injector temperature (°C)	100
Detector temperature (°C)	150
Current (mA)	-
Analysed gas	Hydrocarbon C ₁ -C ₄

สถาบันวิทยบริการ
จุฬาลงกรณ์มหาวิทยาลัย

CHAPTER V

RESULTS AND DISCUSSION

This chapter is divided into two major parts. In the first part, the catalyst characterizations using XRD and nitrogen physisorption are described. And the kinetic modeling of the photocatalytic oxidation of ethylene over titanium dioxide is presented in the last part.

5.1 Characterization of the catalysts

The catalyst in this experiment was prepared via a sol-gel method and was calcined at 350 °C for 3 hours. The bulk crystalline phases of the sample were determined using X-ray diffractometry (XRD). The XRD pattern of TiO₂ is shown in Figure 5.1. The dominant peaks of anatase were observed at 2θ of about 25.2°, 37.9°, 47.8°, and 53.8°, which represent the indices of (101), (004), (200), and (105) planes, respectively. Rutile phase was also identified by a dominant peak at 2θ of about 27.4°, which represented the index of (110) plane. Therefore, the sample was the combination of anatase and rutile phases. Average crystallite size was calculated from the line broadening of (110) diffraction peak using the Scherrer formula. The crystallite size of anatase was approximately 5 nm. But crystallite size of rutile could not be determined because the observed rutile peaks were too small.

สถาบันวิทยบริการ
จุฬาลงกรณ์มหาวิทยาลัย

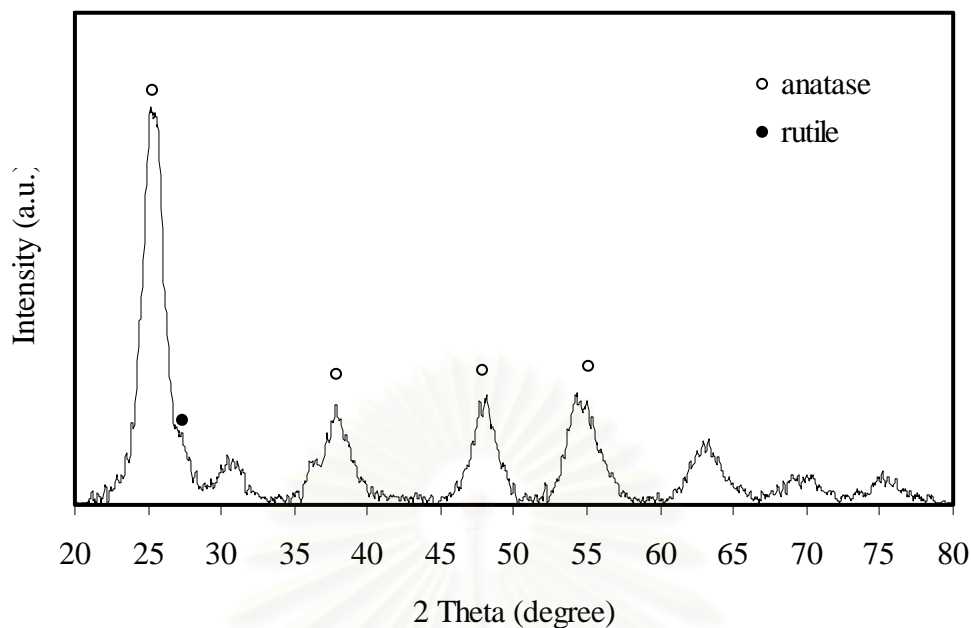


Figure 5.1 XRD patterns of titania calcined at 350 °C for 3 hours.

The BET surface areas of titania was determined by nitrogen adsorption technique. The samples exhibited reasonably high specific surface area of 134 m² g⁻¹.

5.2 Kinetic modeling of the photocatalytic oxidation of ethylene

In this research, the photocatalytic oxidation of ethylene in the gas phase over titanium dioxide was studied. The overall reaction scheme of the oxidation of ethylene is shown below:



The effects of three reaction parameters, namely, flow rate of reactant, humidity level, and temperature, on the kinetics of the photocatalytic oxidation process were investigated.

5.2.1 The design equation for the pack bed reactor

The pack bed reactor was used as a photoreactor. In order to develop the design equation for the reactor, several assumptions for a plug flow reactor were made: (1) the concentration varies continuously in the axial direction through the reactor; (2) the flow is highly turbulent; (3) there is no radial variation in the concentration, temperature or reaction rate; and (4) the reactor operates at steady state (Fogler, 1999). One could begin the derivation a mole balance on species A over the differential reactor volume. The assumption of a plug flow reactor and a homogeneous reaction led to the design equation shown in Equation 5.2:

$$\frac{dF_A}{dV} = r_A \quad (5.2)$$

where F_A is the molar flow rate of the reactant A , V is the volume of the reactor, r_A is the rate of reaction for reactant A . In a gas-solid heterogeneous system, the rate of reaction for a substance A can be defined as

$$r'_A = \text{mole of } A \text{ reacted}/(\text{time})(\text{weight of catalyst})$$

The weight of catalyst is used instead of reactor volume because the amount of the catalyst is more important to the rate of reaction than the reactor volume. The derivation of the design equation for a pack bed reactor is carried out on a manner analogous to the development of the design equation for a tubular reactor.

$$\frac{dF_A}{dW} = r'_A \quad (5.3)$$

When pressure drop through the reactor and catalyst deactivation are neglected, the integral form of the pack bed design equation can be used to calculate the catalyst weight.

$$W = \int_{F_{A0}}^{F_A} \frac{dF}{r'_A} \quad (5.4)$$

For a flow system, F_A has been given in terms of the entering molar flow rate F_{A0} and conversion X :

$$F_A = F_{A0} - F_{A0}X \quad (5.5)$$

Substituting of Equation 5.5 into Equation 5.3 gives the different form of the design equation for pack bed reactor:

$$F_{A0} \frac{dX}{dW} = -r'_A \quad (5.6)$$

Integrating with the limit of $W = 0$ when $X = 0$ and a specified conversion X :

$$\frac{W}{F_{A0}} = \int_0^X \frac{dX}{-r'_A} \quad (5.7)$$

where W is the weight of the catalyst and $-r'_A$ is the rate of disappearance of reactant A per unit weight of catalyst.

The fractional conversion of A , X_A , is the number of moles of A that have reacted per mole of A fed to the system:

$$X_A = \frac{\text{moles of } A \text{ reacted}}{\text{moles of } A \text{ fed}} \quad (5.8)$$

The conversion is determined from the following relation:

$$X_A = \frac{N_{A0} - N_A}{N_{A0}} = 1 - \frac{N_A}{N_{A0}} \quad (5.9)$$

where N_{A0} is the initial number of mole of reactant A and N_A is the number of mole of reactant A at any time. Rearranging of Equation 5.9 gives

$$N_A = N_{A0}(1 - X_A) \quad (5.10)$$

When the number of moles of product equals the number of moles of reactant at the same temperature and pressure, the volume of the reacting mixture will not change ($V = V_0$) if the compressibility factors of the products and reactants are approximately equal. The concentration of A is the number of mole A per unit volume:

$$C_A = \frac{N_A}{V} = \frac{N_A}{V_0} = \frac{N_{A0}(1 - X_A)}{V_0} = C_{A0}(1 - X_A) \quad (5.11)$$

where V_0 is the initial volume of reactant A, C_{A0} is the concentration of reactant A corresponding to zero conversion.

To determine the number of mole of species i remaining after $N_{A0}X_A$ moles of A have reacted, one use the stoichiometric to express the total number of mole of i that have reacted is

$$\begin{aligned} \text{moles } i \text{ reacted} &= \frac{\text{moles } i \text{ reacted}}{\text{moles } A \text{ reacted}} \cdot (\text{moles } A \text{ reacted}) \\ &= \frac{\nu_i}{\nu_A} (N_{A0}X_A) \end{aligned} \quad (5.12)$$

where ν_i and ν_A represent the stoichiometric coefficient of species i and A, respectively. The number of mole of i remaining in the system, N_i , is given in Equation 5.13

$$N_i = N_{i0} - \frac{\nu_i}{\nu_A} N_{A0}X_A \quad (5.13)$$

where N_{i0} is the number of moles initially in the system. The negative sign indicates that i is disappearing from the system. If there is no volume change, one can express the concentration of species i :

$$C_i = \frac{N_i}{V} = C_{i0} - \frac{\nu_i}{\nu_A} \cdot C_{A0} \cdot X_A \quad (5.14)$$

5.2.2 Statistical methods for analysis of kinetic data

The data were fitted by using nonlinear regression analyses. Athena Visual Studio was used to solve the design equation and optimizes nonlinear kinetic parameters in the kinetic models. Linearization of nonlinear models was employed to determine the initial estimates of the nonlinear parameters because nonlinear regression analysis required good initial estimates for the parameters in the model

The operating conditions used to collect the kinetic data for the photocatalytic oxidation of ethylene were shown in Table 5.1. The entering molar flow rate of ethylene can be determined from the following relation:

$$F_{A0} = \nu_0 \cdot C_{A0} \quad (5.15)$$

where F_{A0} is the entering molar flow rate of ethylene, ν_0 is the entering volumetric flow rate and C_{A0} is the entering concentration of ethylene. The volumetric flow rate was measured using a bubble flow meter and the ideal gas law was used to calculate the entering concentration of ethylene.

Table 5.1 Operating conditions for experimental set

Operating parameter	Operating range
Flow rate (ml/min)	3-150
Temperature (°C)	90-50
Relative humidity (%)	0-100
Ethylene content (% v/v)	0.1

5.2.3 Kinetic models for photocatalytic oxidation of ethylene.

Langmuir-Hinshelwood-Hougen-Watson (LHHW) model is a well-known reaction model employed to discuss photocatalytic reactions (Wu *et al.*, 2005). For a surface-catalyzed reaction, Langmuir first developed the adsorption isotherm that lead to a uni-molecular layer of adsorbed molecules. Two assumptions were made: (1) the heat of adsorption is the same for every molecule, and (2) every molecule that strikes a molecule already adsorbed returns immediately to the gas phase. Hinshelwood began the application of Langmuir isotherms to the various reactants and products (Zhao and Yang, 2005). The model developed was thus called Langmuir-Hinshelwood kinetic model. Moreover, Langmuir-Hinshelwood model was popularized by Houngen and Watson and occasionally their names were included (Fogler, 1999).

The form of this LHHW model is presented below

$$-r_A = k_A \cdot \theta_A = \frac{k_A \cdot K_A \cdot P_A}{1 + K_A \cdot P_A} \quad (5.16)$$

where θ_A is fractional surface coverage of ethylene; k_A is the rate constant [$mol/(g \cdot s)$]; K_A denotes the adsorption equilibrium constant for ethylene [Pa^{-1}]. The gaseous influent was assumed to be ideal gas because the total pressure in the reactor was used only about 20 psi greater than an atmospheric pressure. The ideal gas law can be written in terms of the partial pressure of ethylene as

$$P_A = \frac{N_A RT}{V} = \frac{N_{A0} RT(1 - X_A)}{V} = P_{A0}(1 - X_A) \quad (5.17)$$

where R is the gas constant, T is the absolute temperature, V is volume (which does not change because there is no change in number of moles for the oxidation of ethylene), and P_{A0} is the partial pressure of ethylene at the entrance of the reactor. Substituting Equation 5.17 into Equation 5.16 gives

$$-r_A = \frac{k_A K_A P_{A0}(1 - X_A)}{1 + K_A P_{A0}(1 - X_A)} \quad (5.18)$$

This LHHW rate expression can then be substituted into the design equation for plug flow reactor (Equation 5.7). Integration of the right hand side of the equation gives

$$\frac{W}{F_{A0}} = \frac{-1}{k_A K_A P_{A0}} \cdot \ln(1 - X_A) + \frac{1}{k_A} \cdot X_A \quad (5.19)$$

Initial estimates of the two parameters, i.e., k_A and K_A , can be obtained from linear regression analysis of appropriate linearization of the nonlinear model (see Appendix A).

5.2.4 Effect of water vapor on the photocatalytic oxidation of ethylene

The effect of water vapor on the photocatalytic oxidation of ethylene was investigated. Water vapor was added to the feed stream through a water saturator. A portion of the reactant gas was passed through a water saturator that served to saturate this gas with water. The humid stream was then recombined with the dry stream and the combined stream entered the photoreactor in order to obtain the desired level of humidity in the feed. The concentration of water vapor in the stream could be calculated using the vapor pressure of water at the measured temperature of the saturator that was determined from Antoine equation (see Appendix B).

Kinetic data were collected for experiments involving different concentrations of water in the feed. The reaction was performed at 90 °C. The data were modeled using a first-order LHHW rate expression. The corresponding kinetic parameters are summarized in Table 5.2. Kinetic data and the best fit curves determined from nonlinear regression analysis at various relative humidities, namely, 0%, 20%, 40%, 60%, 80%, and 100%, and are shown in Figures 5.2, 5.3, 5.4, 5.5, 5.6, and 5.7, respectively. Figure 5.8 illustrates how water vapor affects the photocatalytic reaction rates of ethylene. The reaction rates of ethylene decreased with increasing water vapor concentration probably due to competitive adsorption between water and ethylene on the surface of the catalyst.

Table 5.2 Parameter estimates obtained from nonlinear regression analysis of kinetic data obtained at various relative humidities using a first-order LHHW rate expression. The temperature of the reaction is 90 °C.

Relative humidity (%RH)	Parameter estimation \pm 95% confidence interval	
	k_A (mol/g·s)	K_A (Pa ⁻¹)
0	$1.80 \times 10^{-7} \pm 2.59 \times 10^{-7}$	$2.35 \times 10^{-3} \pm 6.40 \times 10^{-3}$
20	$1.58 \times 10^{-7} \pm 1.06 \times 10^{-7}$	$1.91 \times 10^{-3} \pm 1.65 \times 10^{-3}$
40	$4.32 \times 10^{-8} \pm 1.00 \times 10^{-8}$	$1.11 \times 10^{-2} \pm 5.92 \times 10^{-3}$
60	$3.72 \times 10^{-8} \pm 1.07 \times 10^{-8}$	$1.23 \times 10^{-2} \pm 9.61 \times 10^{-3}$
80	$3.49 \times 10^{-8} \pm 1.28 \times 10^{-8}$	$1.40 \times 10^{-2} \pm 1.35 \times 10^{-2}$
100	$2.79 \times 10^{-8} \pm 3.77 \times 10^{-9}$	$2.65 \times 10^{-2} \pm 1.42 \times 10^{-2}$

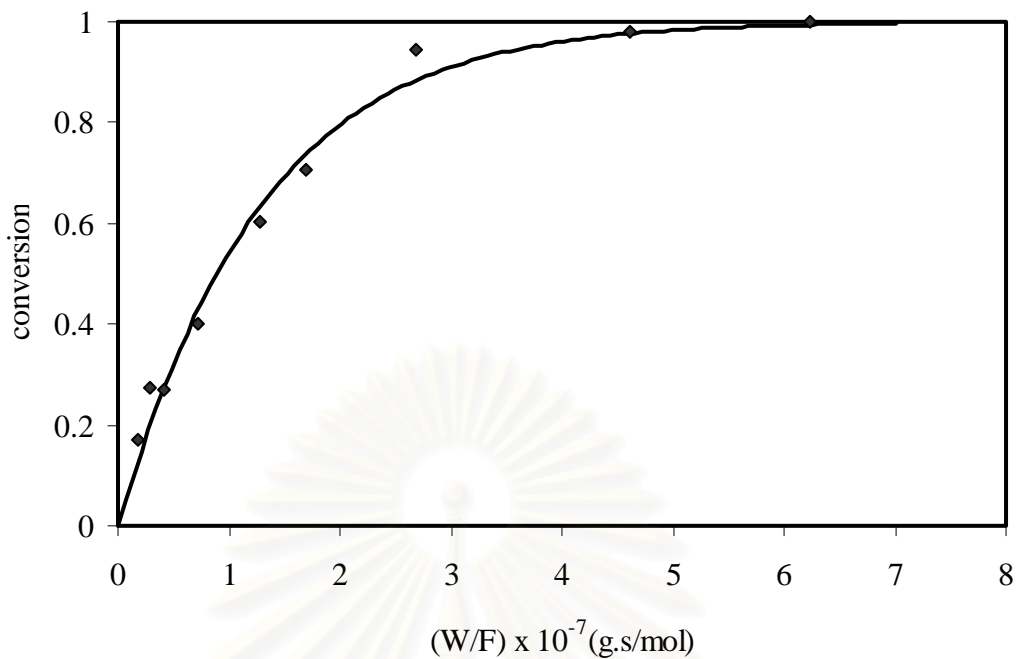


Figure 5.2 Kinetic data for the photocatalytic oxidation of ethylene at 90 °C. The relative humidity is 0%. The line corresponds to the best fit curve determined from nonlinear regression analysis of the data in terms of a first-order LHHW rate expression.

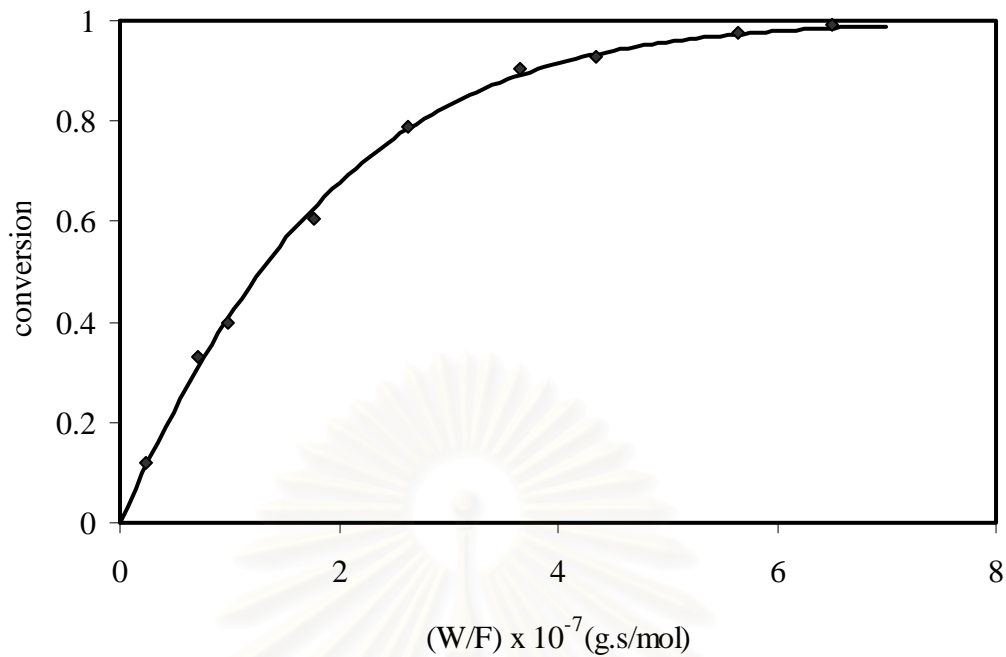


Figure 5.3 Kinetic data for the photocatalytic oxidation of ethylene at 90 °C. The relative humidity is 20%. The line corresponds to the best fit curve determined from nonlinear regression analysis of the data in terms of a first-order LHHW rate expression.

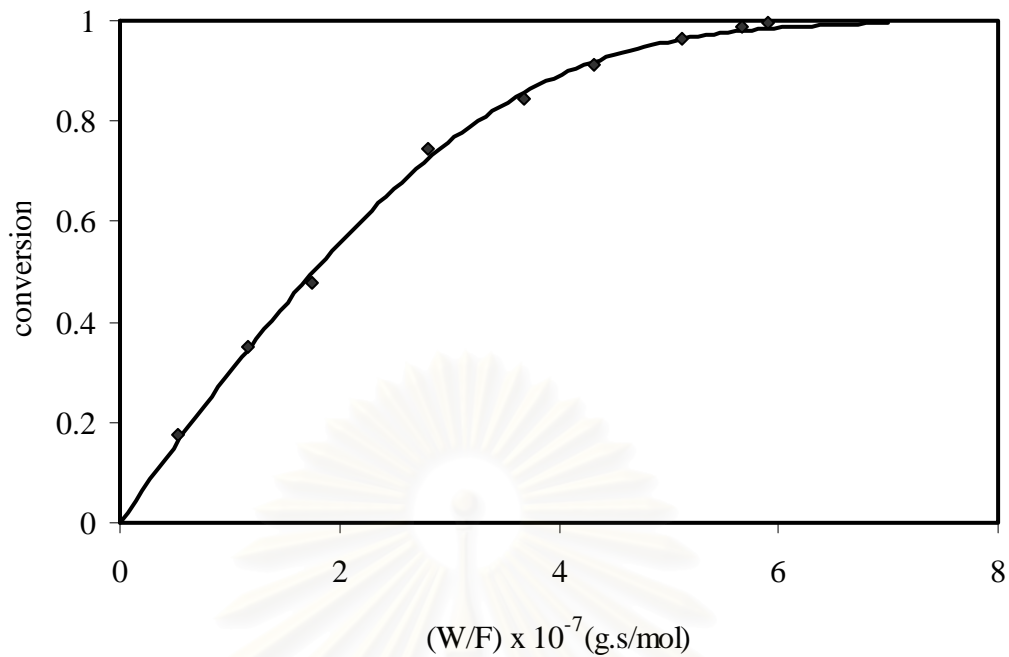


Figure 5.4 Kinetic data for the photocatalytic oxidation of ethylene at 90 °C. The relative humidity is 40%. The line corresponds to the best fit curve determined from nonlinear regression analysis of the data in terms of a first-order LHHW rate expression.

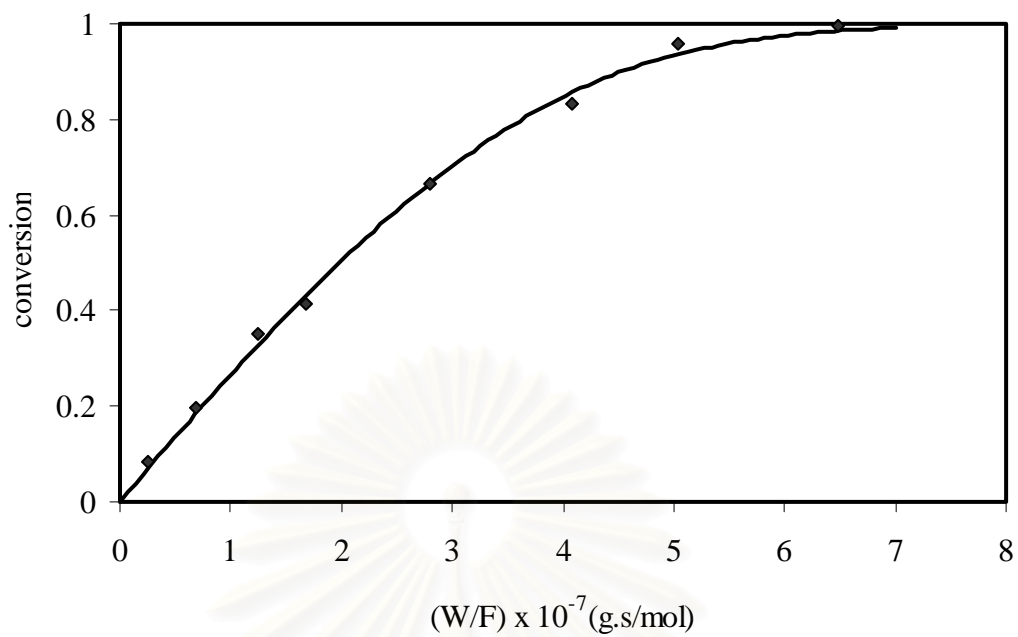


Figure 5.5 Kinetic data for the photocatalytic oxidation of ethylene at 90 °C. The relative humidity is 60%. The line corresponds to the best fit curve determined from nonlinear regression analysis of the data in terms of a first-order LHHW rate expression.

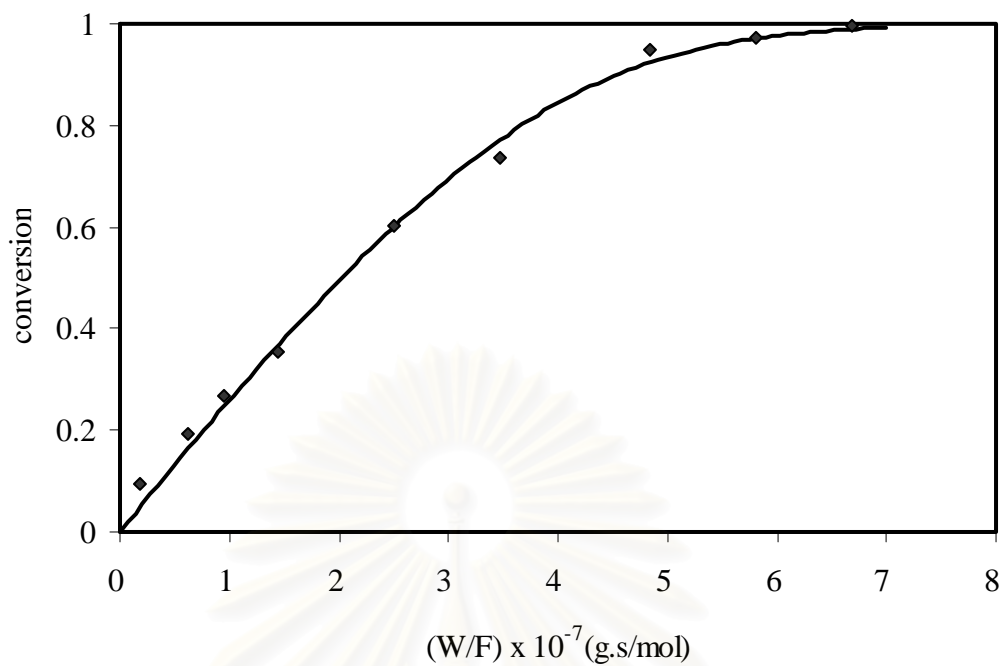


Figure 5.6 Kinetic data for the photocatalytic oxidation of ethylene at 90 °C. The relative humidity is 80%. The line corresponds to the best fit curve determined from nonlinear regression analysis of the data in terms of a first-order LHHW rate expression.

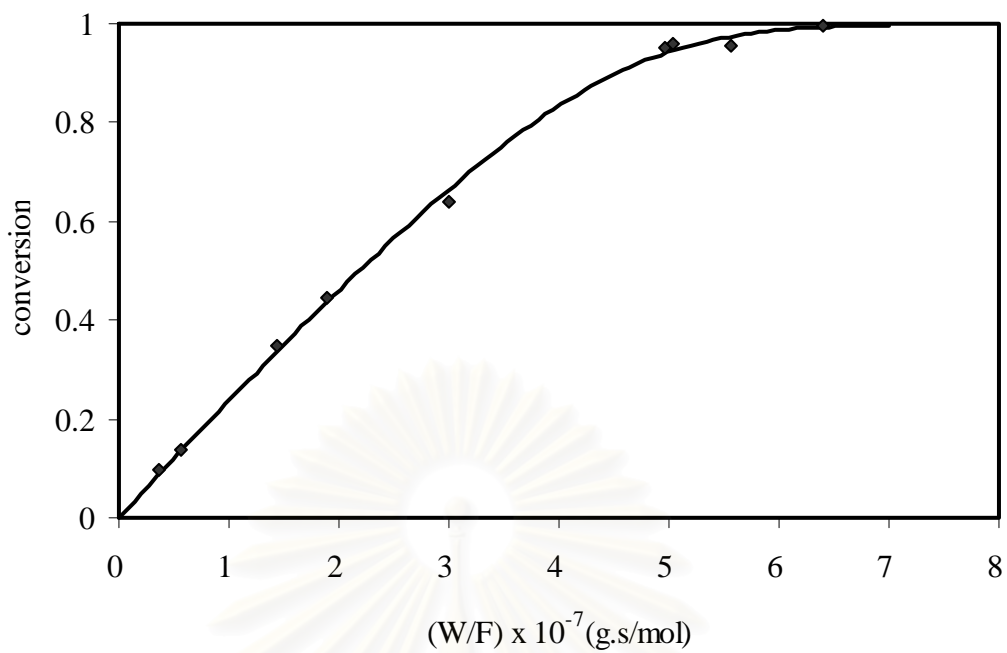


Figure 5.7 Kinetic data for the photocatalytic oxidation of ethylene at 90 °C. The relative humidity is 100%. The line corresponds to the best fit curve determined from nonlinear regression analysis of the data in terms of a first-order LHHW rate expression.

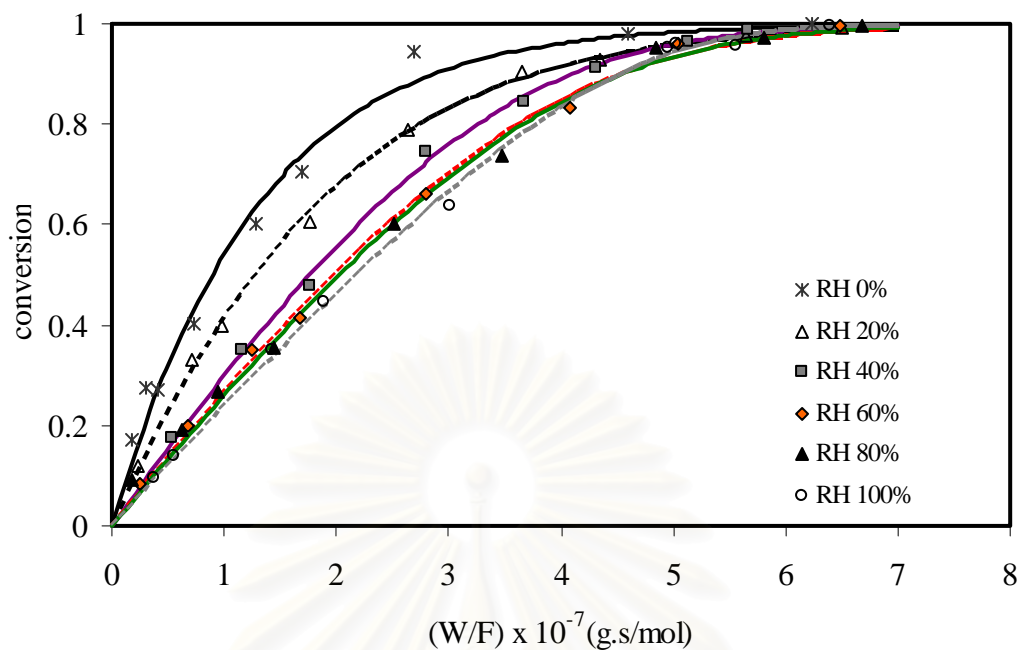


Figure 5.8 Kinetic data for the photocatalytic oxidation of ethylene at various relative humidities. The temperature of the reaction is 90 °C. The lines correspond to the best fit curves as determined from nonlinear regression analysis of the data using a first-order LHHW rate expression.

5.2.4.1 Incorporation of concentration of water in the kinetic model

The photocatalytic oxidation of ethylene involves the surface reaction between ethylene and oxygen species. The overall reaction scheme of the oxidation of ethylene can be expressed as:



The equilibrium constant was used to assess the reversibility of the reaction. One could calculate such constant from Gibbs free energy of formation (ΔG_f^0) and Enthalpies of formation (ΔH_f^0), which are listed in Table 5.3.

Table 5.3 Enthalpy of formation and Gibbs free energy of formation at 25 °C, 1 atm

Substance	ΔH_f^0 (kJ/mol)	ΔG_f^0 (kJ/mol)
C ₂ H ₄	52.47	68.42
O ₂	0	0
CO ₂	-393.52	-394.39
H ₂ O	-241.83	-228.52

Source: Saad, M. A., *Thermodynamics Principles and Practice*, Prentice-Hall, Inc., New Jersey, 1997, pp. 605.

The change in Gibbs free energy of formation for the reaction was calculated using the relation

$$\Delta G_{Rx}^0 = \sum_i (\nu_i \cdot \Delta G_{f,i}^0) \quad (5.20)$$

$$= 2(-394.39) + 2(-228.52) - 68.42 - 3(0)$$

$$\Delta G_{Rx}^0 = -1314.24 \text{ kJ/mol}$$

The equilibrium constant at 298.15 K was then calculated from the change in the Gibbs free energy using

$$RT \ln K = -\Delta G_{Rx}^0 \quad (5.21)$$

$$\ln K = \frac{-\Delta G_{Rx}^0}{RT} = \frac{-(-1314.24 \text{ kJ/mol})}{8314.34 \text{ mol/kg} \cdot \text{mol} \cdot \text{K} (298.15 \text{ K})} = 530.17$$

$$K = 1.78 \times 10^{230} \text{ at } 298.15 \text{ K}$$

And the equilibrium constant at the reaction temperature (90 °C or 363.15 K) was determined from

$$\ln\left(\frac{K_1}{K_2}\right) = \frac{\Delta H_{Rx}^0}{R} \left(\frac{1}{T_1} - \frac{1}{T_2}\right) \quad (5.22)$$

where the standard enthalpy change for the reaction was assumed to be constant over temperature range of interest and was calculated using the relation

$$\Delta H_{Rx}^0 = \sum_i (\nu_i \cdot \Delta H_{f,i}^0) \quad (5.23)$$

$$= 2(-393.52) + 2(-241.83) - 52.47 - 3(0)$$

$$\Delta H_{Rx}^0 = -1218.23 \text{ kJ/mol}$$

Substituting Equations 5.21 and 5.23 into Equation 5.22, we obtain

$$\ln\left(\frac{1.78 \times 10^{230}}{K_2}\right) = \frac{-1218.23 \text{ kJ/mol}}{8314.34 \text{ mol/kg} \cdot \text{mol} \cdot \text{K}} \left(\frac{1}{363.15 \text{ K}} - \frac{1}{298.15 \text{ K}}\right)$$

$$K_2 = 1.25 \times 10^{192} \text{ at } 363.15 \text{ K}$$

The equilibrium constant of the reaction at 90 °C is 1.25×10^{192} . Therefore, the reaction is irreversible because the value of the equilibrium constant was very large.

Since the oxidation of ethylene was irreversible, water molecule would not participate in the reaction but compete to adsorb on surface sites. Wang and coworker (1999) proposed that the presence of oxygen would not affect the adsorption of reactants on TiO₂ surface, for which it is assumed here that oxygen and ethylene could be adsorbed on different site. Hence, the rate of reaction can be expressed as (see Appendix C):

$$-r_A = k_A \cdot \theta_{A,I} \cdot \theta_{O,II} = \frac{k_A \cdot K_A \cdot P_A \cdot K_O \cdot P_O}{(1 + K_A \cdot P_A) \cdot (1 + K_O P_O)} \quad (5.24)$$

Where $\theta_{A,I}$ is the fraction of the type *I* sites covered by ethylene and $\theta_{O,II}$ is the fraction of the type *II* sites covered by oxygen. This model was similar to the photocatalytic oxidation of ethylene over thin films of titania supported on glass rings proposed by Sirisuk (2003). Moreover, Yamasaki and coworker (1999) reported that under UV illumination, an electron from valence band on TiO₂ surface jumps to the conduction band and the photoexcited electrons are trapped by Ti^{4+} center to form Ti^{3+} . When O₂ is present, the surface Ti^{3+} is readily oxidized by molecular oxygen to form the superoxide anion. The mechanism is shown below:



Thus, at steady state under UV illumination, Ti^{3+} sites are adsorbed by oxygen while ethylene adsorbs at Ti^{4+} sites.

Using Equations 5.1 and 5.14, one could write equations describing instantaneous partial pressures of water vapor and oxygen as followed:

$$P_W = P_{W0} + 2 \cdot P_{A0} \cdot X_A \quad (5.27)$$

$$P_O = P_{O0} - 3 \cdot P_{A0} \cdot X_A \quad (5.28)$$

where P_w and P_o represent the partial pressures of water vapor and oxygen, respectively; P_{w0} , P_{o0} , and P_{A0} are the initial partial pressures of water, oxygen and ethylene in the influent, respectively; and X_A is the fractional conversion of ethylene.

Three models based on the rate expression in Equation 5.24 were generated to incorporate the effect of the partial pressure of water vapor from the competitive adsorption with other reactants. Each model was described below.

Model 1

Model 1 describes the adsorption of water only on the same type of sites as ethylene. The corresponding rate expression is given by

$$-r_A = \frac{k_A \cdot K_A \cdot P_A \cdot K_O \cdot P_O}{(1 + K_A \cdot P_A + K_W \cdot P_W) \cdot (1 + K_O \cdot P_O)} \quad (5.29)$$

where K_A , K_O and K_W are the adsorption equilibrium constants for ethylene, oxygen and water, respectively.

Model 2

This model represents the adsorption of water only on the same type of sites as oxygen. The corresponding rate expression is can be written as

$$-r_A = \frac{k_A \cdot K_A \cdot P_A \cdot K_O \cdot P_O}{(1 + K_A \cdot P_A) \cdot (1 + K_O P_O + K_w \cdot P_w)} \quad (5.30)$$

Model 3

This model includes the adsorption of water on the both types of sites. The corresponding rate expression is of the form.

$$-r_A = \frac{k_A \cdot K_A \cdot P_A \cdot K_O \cdot P_O}{(1 + K_A \cdot P_A + K_{W,I} \cdot P_W) \cdot (1 + K_O \cdot P_O + K_{W,II} \cdot P_W)} \quad (5.31)$$

where $K_{w,I}$ and $K_{w,II}$ are the adsorption equilibrium constants for water adsorbed on type *I* and type *II* sites, respectively.

The initial estimates for the kinetic parameters were obtained from previous nonlinear regression analysis of the kinetic data using a first-order LHHW rate expression (see Table 5.2). The adsorption equilibrium constant for oxygen was assumed to be equal to that of water.

5.2.4.2 Results of nonlinear regression analyses

Nonlinear regression analyses were employed to fit Models 1, 2, and 3 to the data. The corresponding parameter estimates for all models are shown in Table 5.4. Mean residual sums of squares were employed to compare the three models (see Table 5.5). This result indicates that the best fit is Model 1. Since Models 1 and 2 are nested within Model 3, an extra sum of squares test could be performed for each pair of models. The result for first pair, Model 1 and Model 3, is displayed in Table 5.6, while the result for the second pair, Model 2 and Model 3, is displayed in Table 5.7. A p-value of 0.1385 and 0.1428 for the first and second pair, respectively, indicated that Model 3 did not provide an appropriate fit of data at a 95% confidence level. To compare Model 1 with Model 2, the mean residual sum of squares obtained from Model 2 was larger than that obtained from Model 1. Therefore, Model 1 was considered a better model for use in fitting the kinetic data. To assess the quality of the fit, the expected conversion of ethylene calculated from the model was plotted against the conversion of ethylene measured from the experiment. This plot was a straight line at 45° angle, which suggested that Model 1 provided an adequate fitting of the experiment results. Figure 5.10 is a plot of conversion of ethylene as a function of ratio of the weight of catalyst to molar flow rate of ethylene in the influent.

Based on Model 1, water molecules competed for adsorption on the same site as ethylene molecules for the photocatalytic oxidation of ethylene over titanium dioxide. This finding was in agreement with previous studies done by Yamazaki and coworkers (1999) and Obee and Hay (1997).

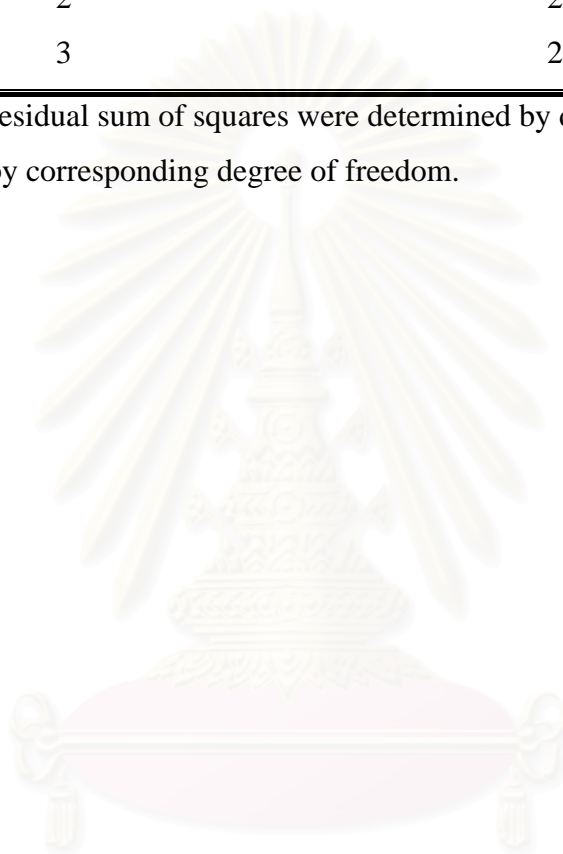
Table 5.4 Parameter estimates obtained from nonlinear regression analysis of kinetic data using Models 1, 2, and 3. The temperature of the reaction is 90 °C.

Model	Parameter	Parameter estimation \pm 95% confidence interval
1	k_A (mol/g·s)	$1.55 \times 10^{-7} \pm 1.14 \times 10^{-7}$
	K_A (Pa ⁻¹)	$7.92 \times 10^{-3} \pm 1.13 \times 10^{-2}$
	K_W (Pa ⁻¹)	$4.41 \times 10^{-4} \pm 3.74 \times 10^{-4}$
	K_O (Pa ⁻¹)	$1.96 \times 10^{-5} \pm 1.15 \times 10^{-6}$
2	k_A (mol/g·s)	$1.54 \times 10^{-7} \pm 1.07 \times 10^{-7}$
	K_A (Pa ⁻¹)	$8.10 \times 10^{-3} \pm 6.34 \times 10^{-2}$
	K_W (Pa ⁻¹)	$8.93 \times 10^{-4} \pm 7.56 \times 10^{-4}$
	K_O (Pa ⁻¹)	$1.96 \times 10^{-5} \pm 1.06 \times 10^{-6}$
3	k_A (mol/g·s)	$4.96 \times 10^{-7} \pm 1.26 \times 10^{-7}$
	K_A (Pa ⁻¹)	$1.23 \times 10^{-3} \pm 4.70 \times 10^{-3}$
	$K_{W,I}$ (Pa ⁻¹)	1.81×10^{-4}
	$K_{W,II}$ (Pa ⁻¹)	$8.74 \times 10^{-5} \pm 2.77 \times 10^{-4}$
	K_O (Pa ⁻¹)	$1.86 \times 10^{-5} \pm 1.72 \times 10^{-6}$

Table 5.5 Mean residual sums of squares obtained from nonlinear regression analyses of kinetic data using Model 1, 2, and 3. The temperature of the reaction is 90 °C.

Model	Mean residual sum of squares ^a
1	2.3608×10^{-3}
2	2.3635×10^{-3}
3	2.5952×10^{-3}

Note: a. Mean residual sum of squares were determined by dividing residual sum of squares by corresponding degree of freedom.



สถาบันวิทยบริการ
จุฬาลงกรณ์มหาวิทยาลัย

Table5.6 Result of extra sum of squares test performed for Model 1 and Model 3

Source	Residual sum of squares	Degrees of freedom	Mean residual sum of squares	F-ratio ¹	p-value ²
Extra	5.89×10^{-3}	1	5.89×10^{-4}	2.27	0.1385
Model 3	1.2157×10^{-1}	48	2.5952×10^{-3}		
Model 1	1.1568×10^{-1}	49			

Note: 1. The F-ratio is the ratio of the extra mean sum of squares to the sum of squares of the full model.

2. A p-value less than 0.05 indicate that at 95% confidence level the model with fewer degrees of freedom should be selected.

Table5.7 Result of extra sum of squares test performed for Model 2 and Model 3

Source	Residual sum of squares	Degrees of freedom	Mean residual sum of squares	F-ratio ¹	p-value ²
Extra	5.76×10^{-5}	1	5.76×10^{-5}	2.22	0.1428
Model 3	1.2157×10^{-1}	48	2.5952×10^{-3}		
Model 2	1.1581×10^{-1}	49			

Note: 1. The F-ratio is the ratio of the extra mean sum of squares to the sum of squares of the full model.

2. A p-value less than 0.05 indicate that at 95% confidence level the model with fewer degrees of freedom should be selected.

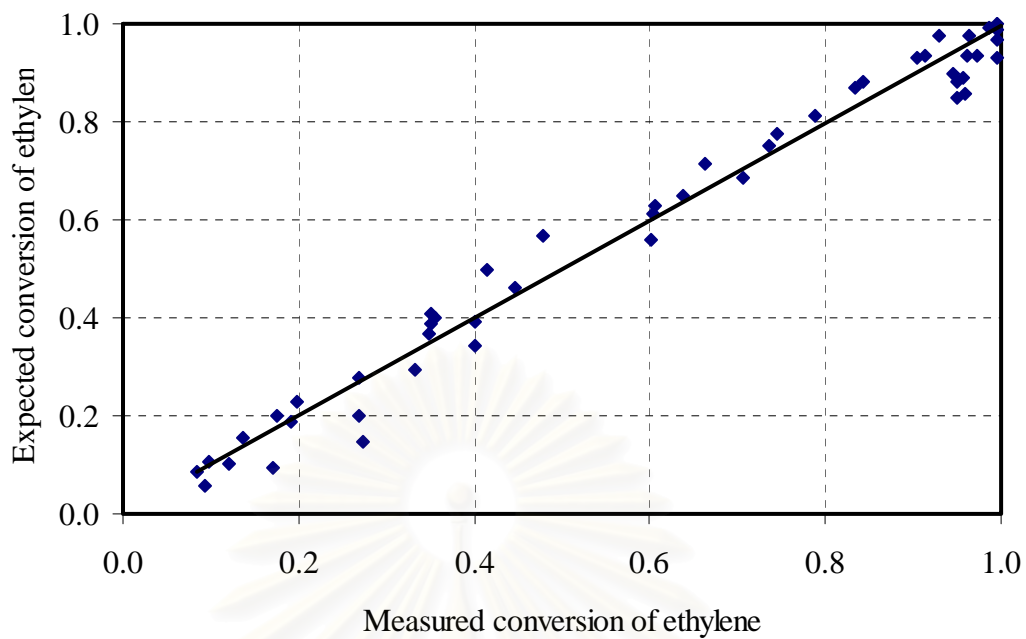


Table 5.9 Plot of the expected conversion of ethylene versus the conversion measured from the experiments for photocatalytic oxidation of ethylene. The line corresponding to $y = x$ is included as reference.

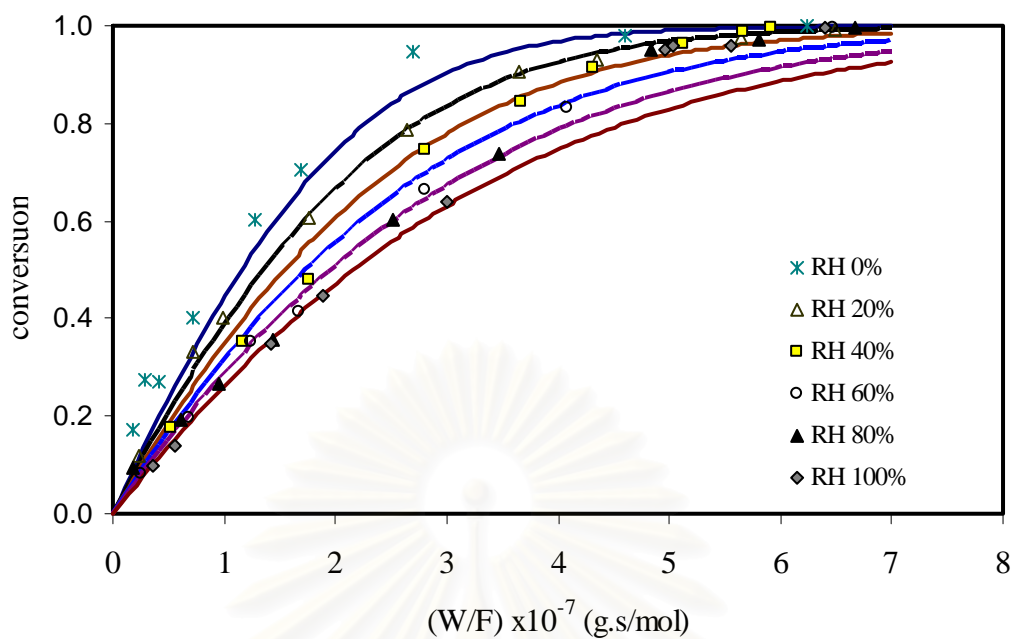


Table 5.10 Kinetic data for the photocatalytic oxidation of ethylene. The temperature is 90 °C. The open circles represent the kinetic data obtained from the experiments. The lines represent the expected conversion determined using nonlinear regression analysis of the data based on Model 1.

5.2.5 Effect of temperature on the photocatalytic oxidation of ethylene

In this part, the effect of temperature on the rate of photocatalytic oxidation of ethylene was investigated by performing at three temperatures and two different concentrations of water vapor in feed stream. At 0% relative humidity, the data were collected at 62, 76, and 90 °C. And the data were collected at 50, 70, and 90 °C at 100% relative humidity. Cooling air is fed to the side of the photoreactor to adjust the temperature to the desired level. The data were fitted by a first-order LHHW rate expression and the estimated parameters at three temperatures are displayed in Tables 5.8 and 5.9 for 0 and 100% relative humidity, respectively. Kinetic data and the best fit curves determined from nonlinear regression analyse of the data for 0% relative humidity at 62, 76, and 90 °C are shown in Figures 5.11, 5.12, and 5.13, respectively. At 100% relative humidity, kinetic data and the best fit curves are shown in Figure 5.15, 5.16, and 5.17 for reaction at 50, 70, and 90 °C, respectively. Figures 5.14 and 5.18 illustrate how temperature affects the photocatalytic reaction rates of ethylene. The reaction rate of ethylene increased with increasing temperatures and the adsorption equilibrium constant decreased with increasing temperature. Wu and coworkers (2005) reported that the rate constant followed an Arrhenius relationship and increased exponentially with temperature. The adsorption of all species on the surface is exothermic, therefore the higher temperature, the smaller the adsorption equilibrium constant (Wu *et al.*, 2005).

From Arrhenius equation, the temperature dependence of the reaction rate could be written as

$$k_A = A \cdot e^{-E_A/RT} \quad (5.32)$$

where A is the preexponential factor or the frequency factor; E_A is the activation energy; R is the gas constant; and T is the absolute temperature. Taking the natural logarithm of Equation 5.32 gives

Table 5.8 Parameter estimates obtained from nonlinear regression analyse of kinetic data obtained at various temperatures based on a first-order LHHW rate expression. The relative humidity is 0%.

Temperature (°C)	Parameter estimation \pm 95% confidence interval	
	k_A (mol/g·s)	K_A (Pa ⁻¹)
62	$9.66 \times 10^{-8} \pm 7.16 \times 10^{-8}$	$3.15 \times 10^{-3} \pm 2.88 \times 10^{-3}$
76	$1.24 \times 10^{-7} \pm 9.04 \times 10^{-8}$	$2.57 \times 10^{-3} \pm 2.20 \times 10^{-3}$
90	$1.80 \times 10^{-7} \pm 2.59 \times 10^{-7}$	$2.35 \times 10^{-4} \pm 6.40 \times 10^{-5}$

Table 5.9 Parameter estimates obtained from nonlinear regression analyse of kinetic data obtained at various temperatures based on a first-order LHHW rate expression. The relative humidity is 100%.

Temperature (°C)	Parameter estimation \pm 95% confidence interval	
	k_A (mol/g·s)	K_A (Pa ⁻¹)
50	$2.09 \times 10^{-8} \pm 2.68 \times 10^{-9}$	$5.30 \times 10^{-2} \pm 4.62 \times 10^{-2}$
70	$2.39 \times 10^{-8} \pm 1.84 \times 10^{-9}$	$3.92 \times 10^{-2} \pm 1.61 \times 10^{-2}$
90	$2.79 \times 10^{-8} \pm 3.77 \times 10^{-9}$	$2.65 \times 10^{-2} \pm 1.42 \times 10^{-2}$

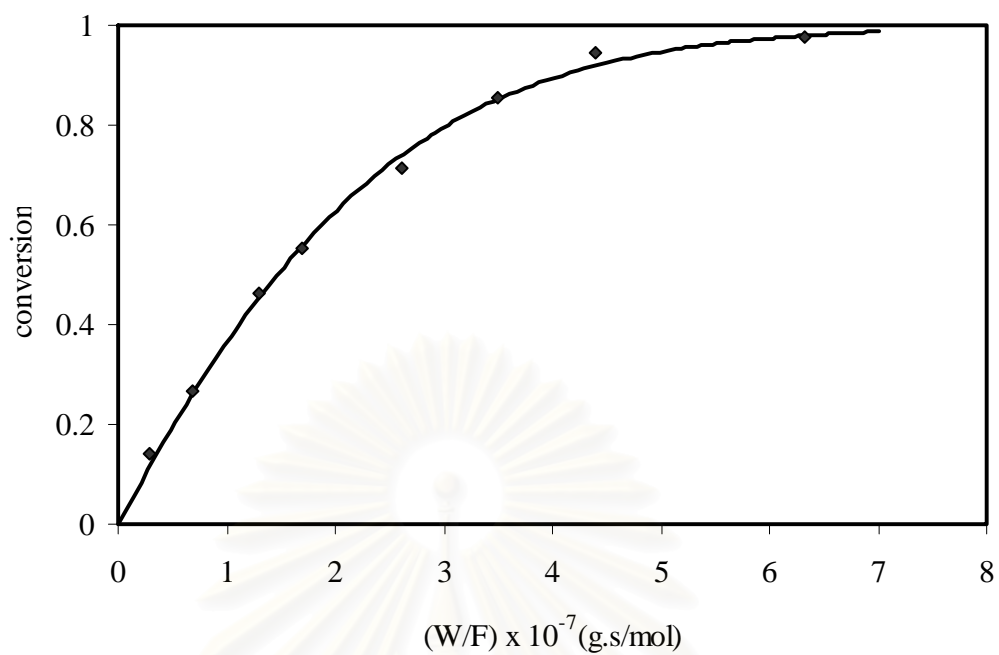


Figure 5.11 Kinetic data for the photocatalytic oxidation of ethylene at 62 °C. The relative humidity is 0%. The line corresponds to the best fit curve determined from nonlinear regression analysis of the data based on a first-order LHHW rate expression.

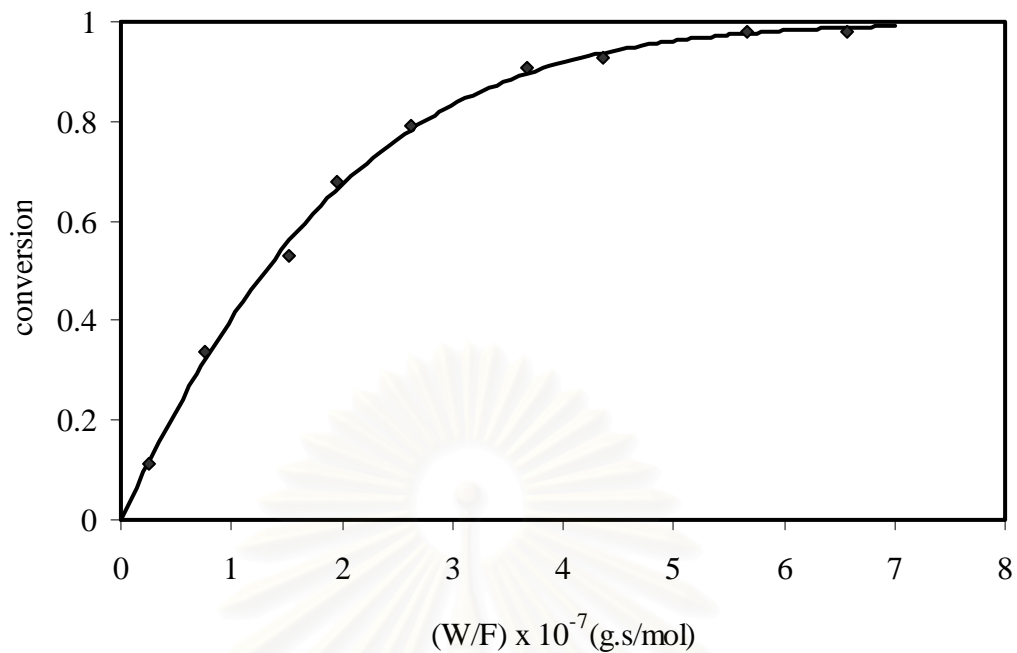


Figure 5.12 Kinetic data for the photocatalytic oxidation of ethylene at 76 °C. The relative humidity is 0%. The line corresponds to the best fit curve determined from nonlinear regression analysis of the data based on a first-order LHHW rate expression.

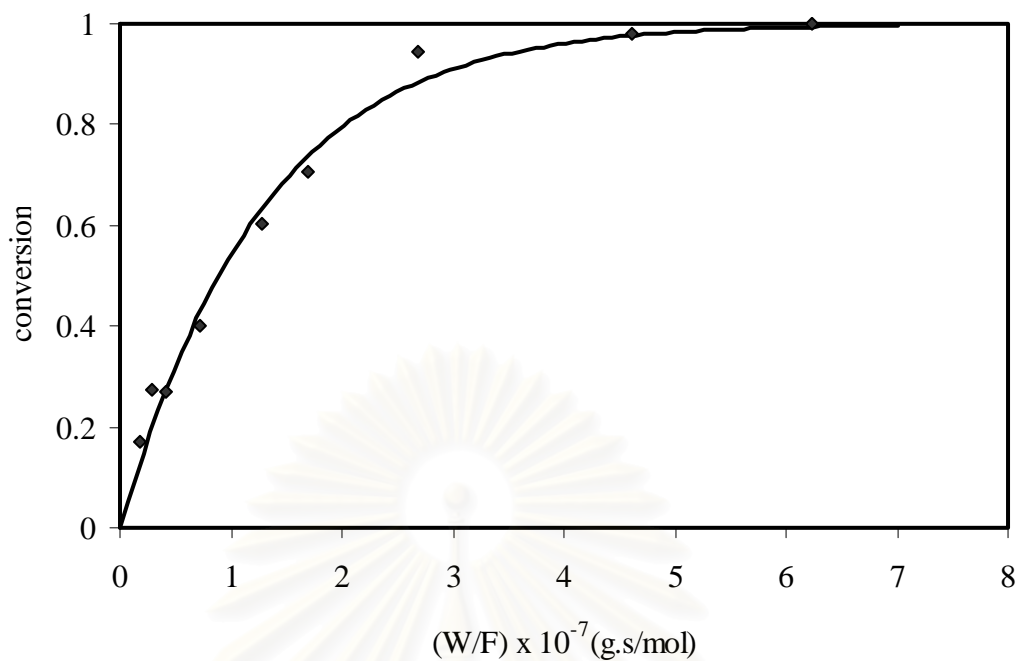


Figure 5.13 Kinetic data for the photocatalytic oxidation of ethylene at 90 °C. The relative humidity is 0%. The line corresponds to the best fit curve determined from nonlinear regression analysis of the data based on a first-order LHHW rate expression.

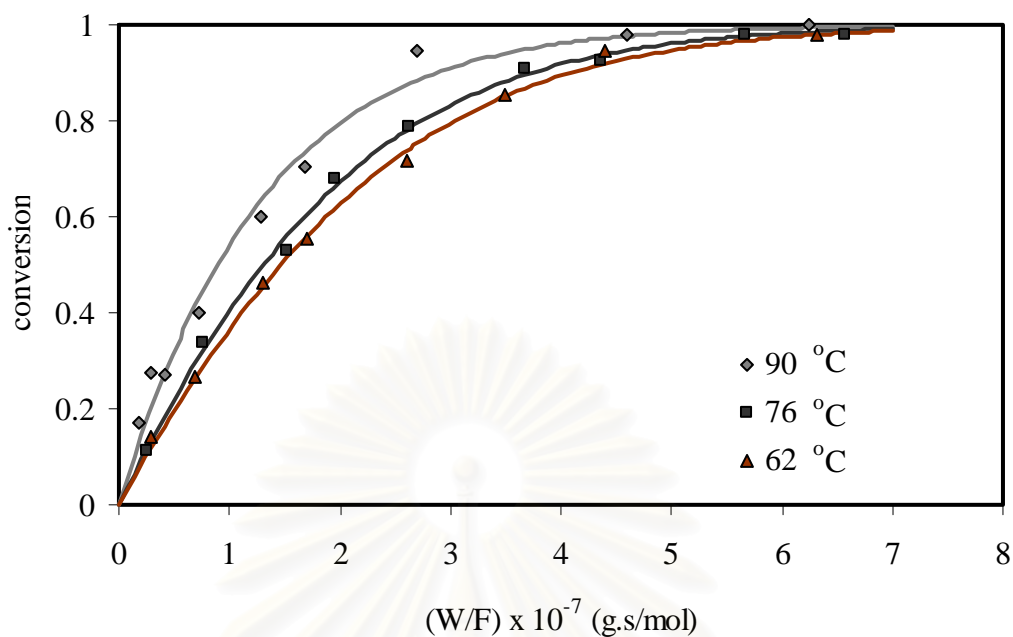


Figure 5.14 Kinetic data for the photocatalytic oxidation of ethylene at three temperatures. The relative humidity is 0%. The lines correspond to the best fit curves determined from nonlinear regression analysis of the data based on a first-order LHHW rate expression.

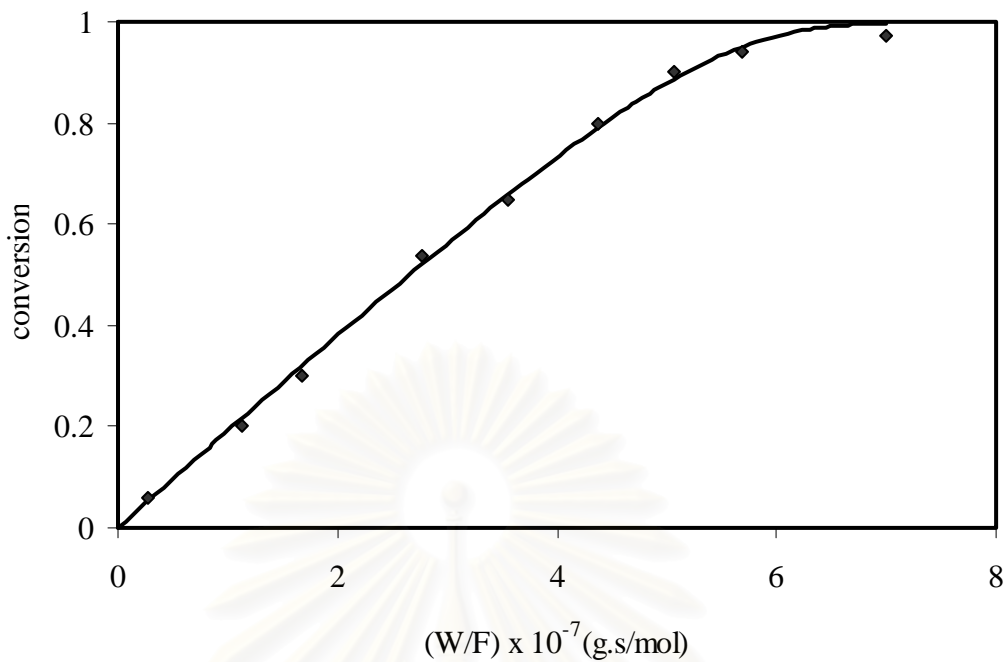


Figure 5.15 Kinetic data for the photocatalytic oxidation of ethylene at 50 °C. The relative humidity is 100%. The line corresponds to the best fit curve determined from nonlinear regression analysis of the data based on a first-order LHHW rate expression.

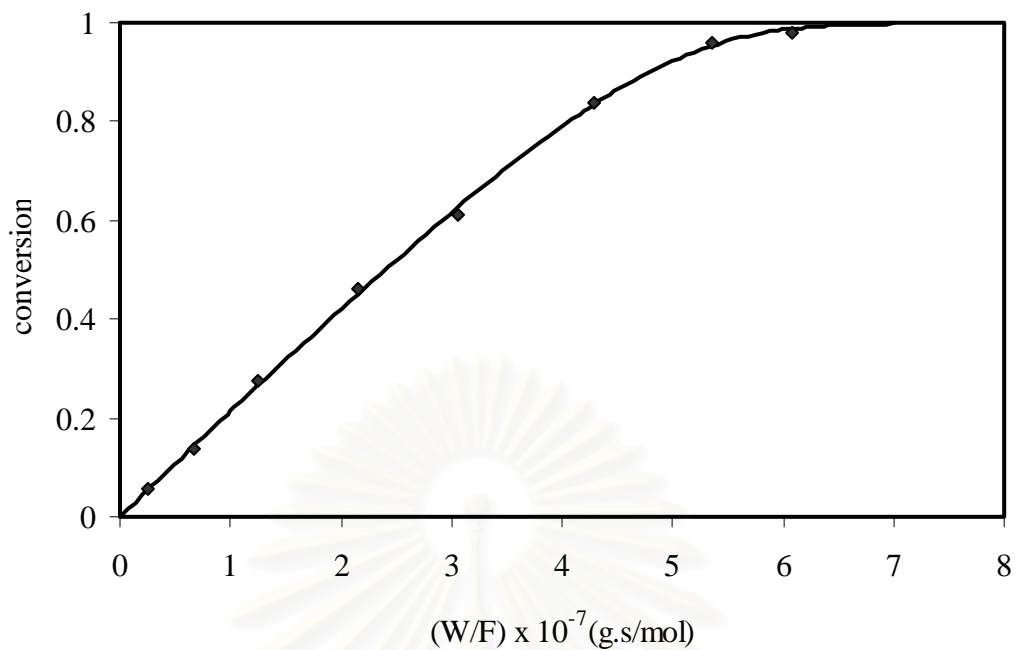


Figure 5.16 Kinetic data for the photocatalytic oxidation of ethylene at 70 °C. The relative humidity is 100%. The line corresponds to the best fit curve determined from nonlinear regression analysis of the data based on a first-order LHHW rate expression.

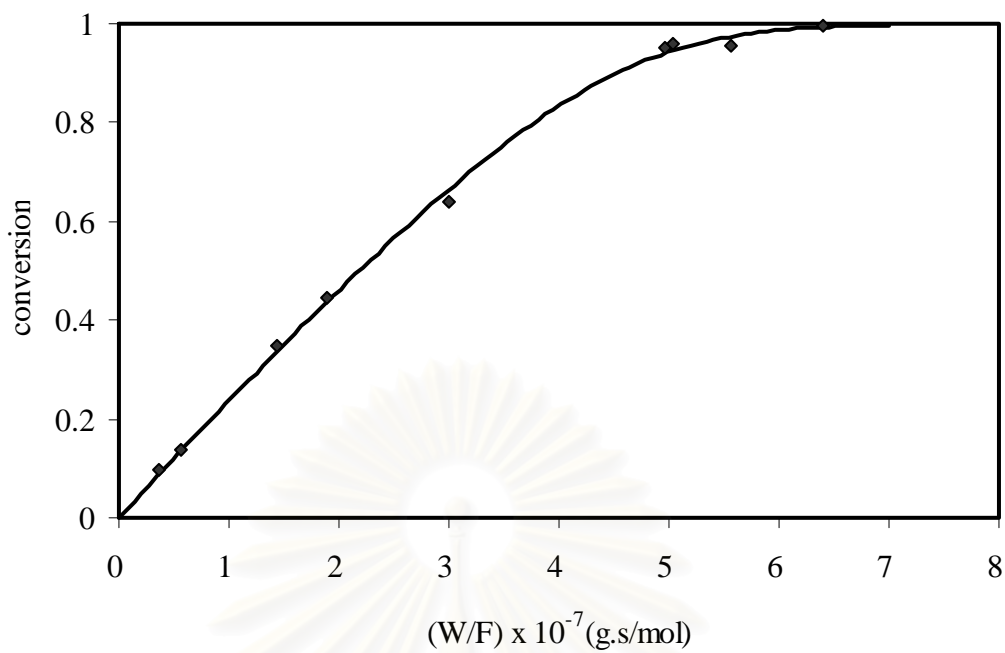


Figure 5.17 Kinetic data for the photocatalytic oxidation of ethylene at 90 °C. The relative humidity is 100%. The line corresponds to the best fit curve determined from nonlinear regression analysis of the data based on a first-order LHHW rate expression.

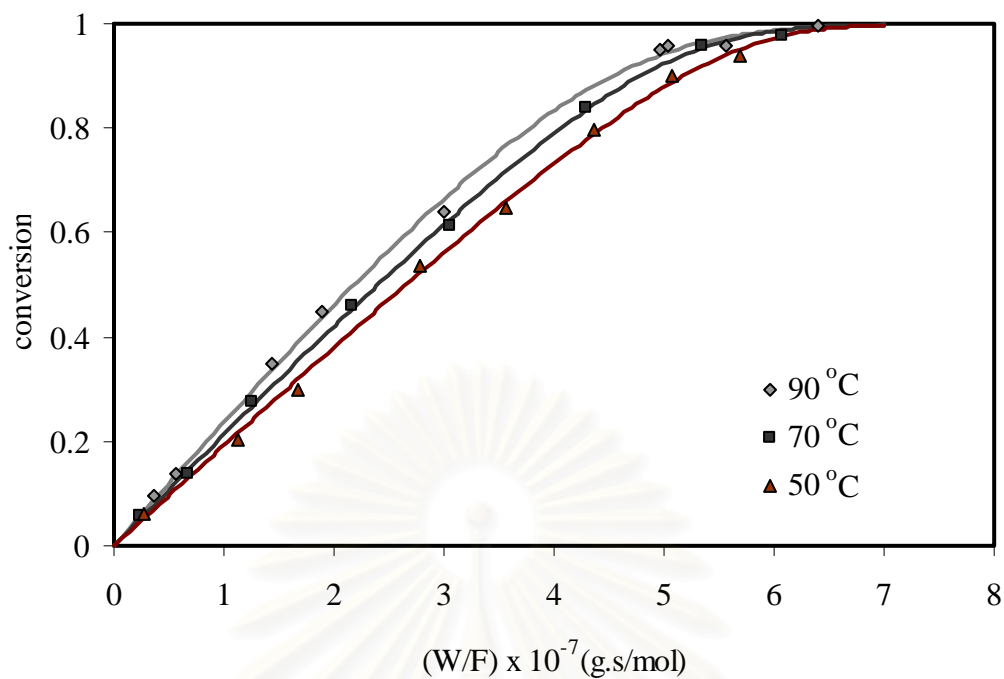


Figure 5.18 Kinetic data for the photocatalytic oxidation of ethylene at three temperatures. The relative humidity is 0%. The lines correspond to the best fit curves determined from nonlinear regression analysis of the data based on a first-order LHHW rate expression.

$$\ln k_A = \ln A - \frac{E_A}{R} \left(\frac{1}{T} \right) \quad (5.33)$$

A plot of $\ln k_A$ versus $1/T$ should be a straight line with the slope of $-(E_A/R)$. Arrhenius equation has been verified empirically to give the temperature behavior of most reaction rate constants within experimental accuracy over fairly large temperature ranges (Fogler, 1999). But in this experiment, the data were obtained in a small range of temperature. Therefore, estimations of activation energies and preexponential factors were highly correlated. In order to reduce the correlation of these estimations, we centered the temperature about an intermediate temperature T_0 as seen in Equation 5.34.

$$\ln k_{A,T} = \ln k_{A,T_0} - \frac{E_A}{R} \left(\frac{1}{T} - \frac{1}{T_0} \right) \quad (5.34)$$

where k_{A,T_0} is the reaction rate constant at an intermediate temperature T_0 .

The apparent enthalpy of adsorption, ΔH_{ads} is related to the equilibrium constant as followed:

$$K_{A,T} = K_{A,T_0} \exp \left[\frac{-\Delta H_{ads}}{R} \left(\frac{1}{T} - \frac{1}{T_0} \right) \right] \quad (5.35)$$

where ΔH_{ads} is the standard enthalpy of adsorption, and K_{A,T_0} is the adsorption equilibrium constant at an intermediate temperature T_0 . Taking the natural logarithm of both sides of Equation 5.35 yields

$$\ln K_{A,T} = \ln K_{A,T_0} - \frac{\Delta H_{ads}}{R} \left(\frac{1}{T} - \frac{1}{T_0} \right) \quad (5.36)$$

The slope of the plot of $\ln K_{A,T}$ as a function of $\left(\frac{1}{T} - \frac{1}{T_0} \right)$ is equal to $-(\Delta H_{ads}/R)$.

The plot of $\ln k_A$ versus $\left(\frac{1}{T} - \frac{1}{T_0}\right)$ and $\ln K_A$ versus $\left(\frac{1}{T} - \frac{1}{T_0}\right)$ are shown in

Figures 5.19a, 5.19b, 5.20a, and 5.20b for 0 and 100% relative humidity, respectively. The activation energy of the reaction and the enthalpy of adsorption for ethylene were determined from multiplying the corresponding negative slopes by the gas constant. The reaction rate constant and the adsorption equilibrium constant at an intermediate temperature T_0 can be calculated from taking the exponential of the corresponding intercept (see Tables 5.10 and 5.11). The activation energies of the reaction were 22.48 and 7.04 kJ/mol for 0 and 100% relative humidity, respectively. The enthalpies of adsorption for ethylene were -11.14 and -16.83 kJ/mol for 0 and 100% relative humidity, respectively.

We can substitute the rate constant (Equation 5.34) and the adsorption equilibrium constant (Equation 5.35) into a LHHW rate expression (Equation 5.16) to obtain the expression

$$-r_A = \frac{k_{A,T_0} \cdot \left\{ \exp \left[\frac{-E_A}{R} \left(\frac{1}{T} - \frac{1}{T_0} \right) \right] \right\} \cdot K_{A,T_0} \cdot \left\{ \exp \left[\frac{-\Delta H_{ads}}{R} \left(\frac{1}{T} - \frac{1}{T_0} \right) \right] \right\} \cdot P_A}{1 + K_{A,T_0} \cdot \left\{ \exp \left[\frac{-\Delta H_{ads}}{R} \left(\frac{1}{T} - \frac{1}{T_0} \right) \right] \right\} \cdot P_A} \quad (5.37)$$

Rearranging give us

$$-r_A = \frac{P_A}{\frac{1}{k_{A,T_0} \cdot K_{A,T_0}} \cdot \exp \left[\frac{(E_A + \Delta H_{ads})}{R} \left(\frac{1}{T} - \frac{1}{T_0} \right) \right] + \left\{ \frac{1}{k_{A,T_0}} \cdot \exp \left[\frac{E_A}{R} \left(\frac{1}{T} - \frac{1}{T_0} \right) \right] \cdot P_A \right\}} \quad (5.38)$$

Nonlinear regression analyses were performed using kinetic data and the parameters that obtained from linear regression (Tables 5.10 and 5.11) were used as the initial guesses. The resulting parameter estimates are presented in Tables 5.12 and 5.13 for 0 and 100% relative humidity, respectively.

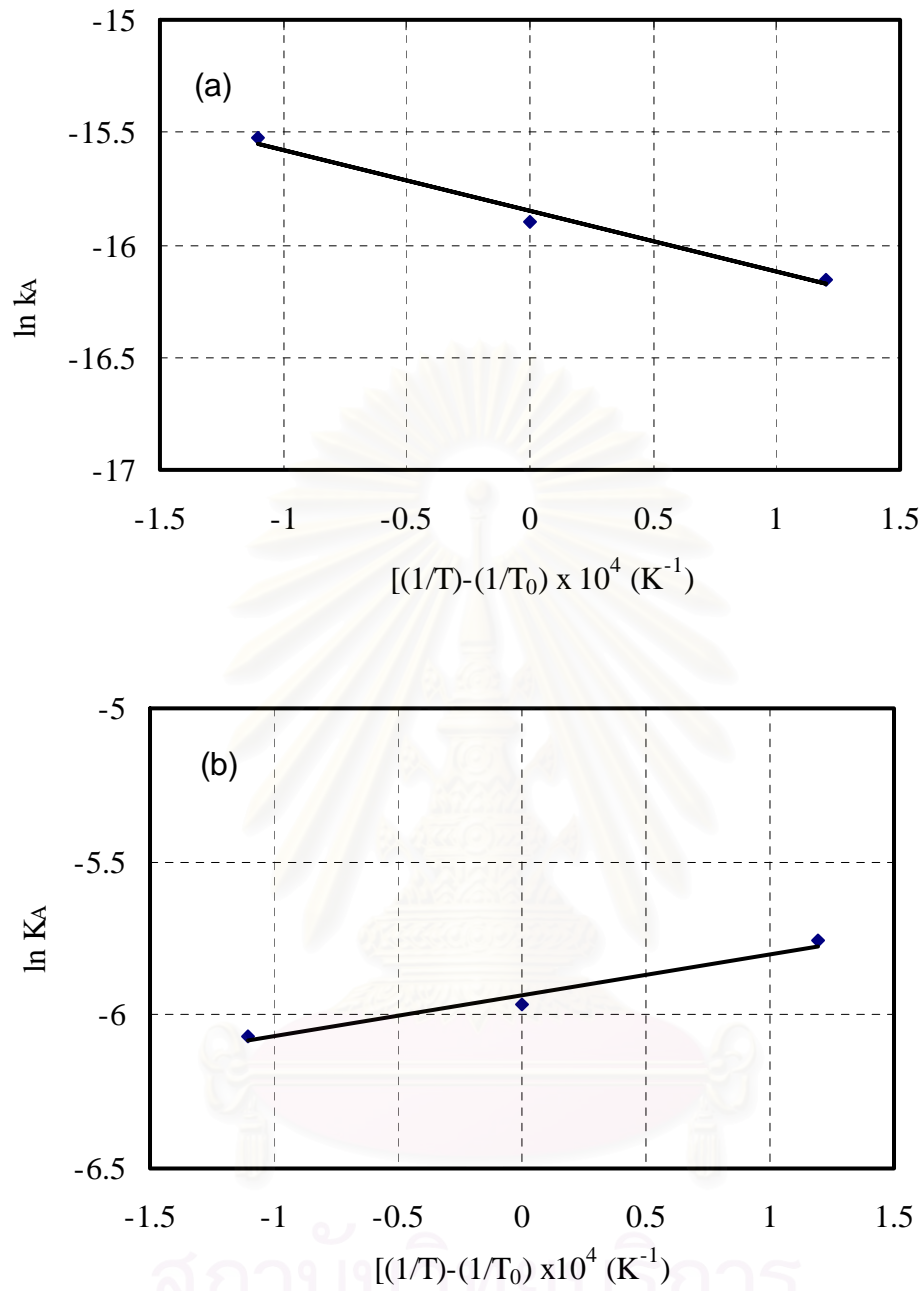


Figure 5.19 (a) Arrhenius plot for rate constants at three temperatures. (b) Arrhenius-type plot for adsorption equilibrium constants obtained at three temperatures. The relative humidity is 0%.

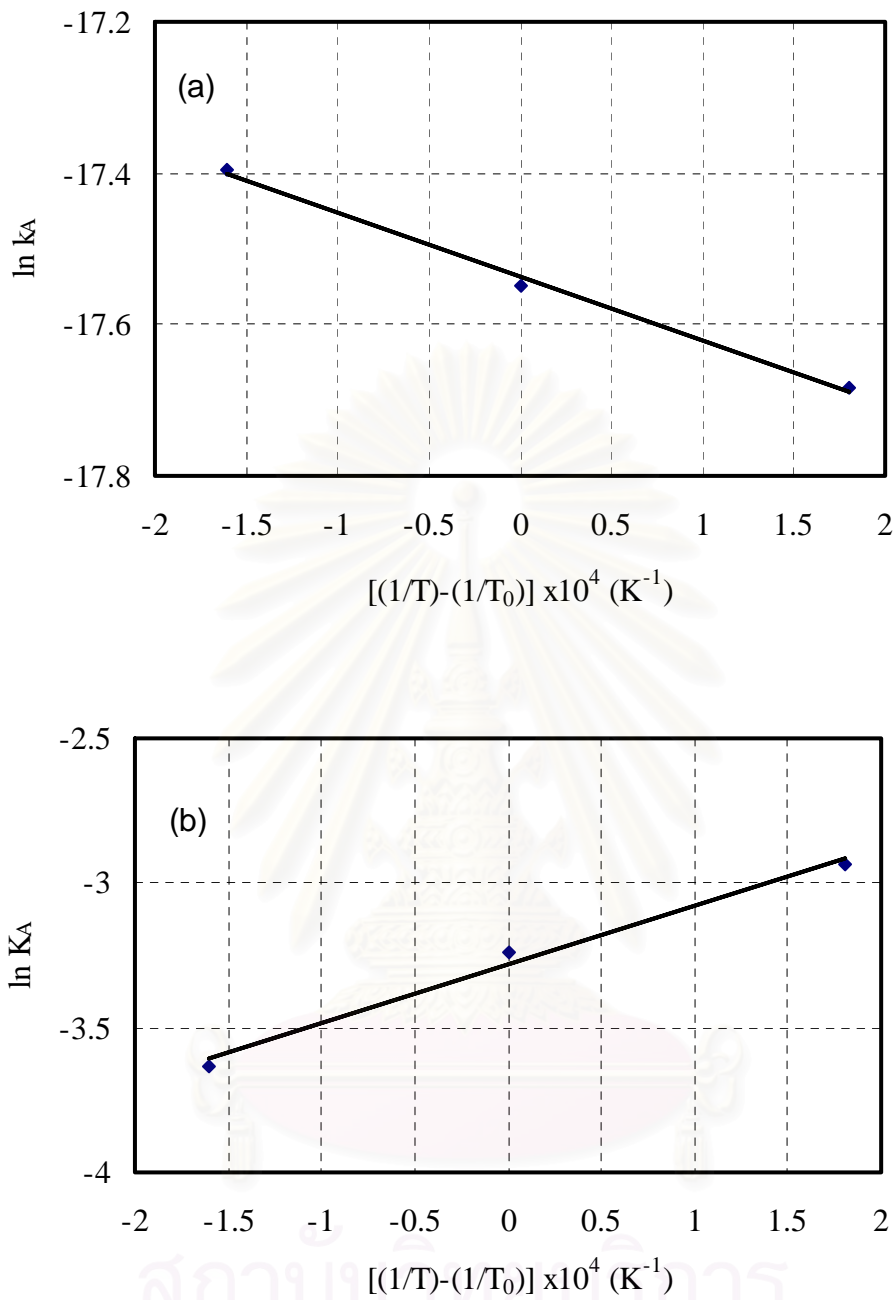


Figure 5.20 (a) Arrhenius plot for rate constants at three temperatures. (b) Arrhenius-type plot for adsorption equilibrium constants obtained at three temperatures. The relative humidity is 100%.

Table 5.10 Parameter estimates obtained from linear regression analyses of an Arrhenius plot for rate constants at three temperatures (Figure 5.19a) and an Arrhenius-type plot for adsorption constants at three temperatures (Figure 5.1b). The relative humidity is 0%. The intermediate temperature (T_0) is 76 °C

	Linear regression parameters		Calculated parameters ^a	
	slope	intercept	$k_A(T_0)$ (mol/g·s)	E_A (kJ/mol)
$\ln k_A$ vs. $\left(\frac{1}{T} - \frac{1}{T_0}\right)$	-2704.00	-15.85	1.31×10^{-7}	22.48
			$K_A(T_0)$ (mol/g·s)	ΔH_{ads} (kJ/mol)
$\ln K_A$ vs. $\left(\frac{1}{T} - \frac{1}{T_0}\right)$	1340.00	-5.93	2.65×10^{-3}	-11.14

Note: a. $k_A(T_0)$ or $K_A(T_0)$ is determined by taking the exponential of the corresponding intercept. E_A or ΔH_{ads} is determined by multiplication the corresponding negative slope with the gas constant

Table 5.11 Parameter estimates obtained from linear regression analyses of an Arrhenius plot for rate constants at three temperatures (Figure 5.20a) and an Arrhenius-type plot for adsorption constants at three temperatures (Figure 5.20b). The relative humidity is 100%.The intermediate temperature (T_0) is 70 °C.

	Linear regression parameters		Calculated parameters ^a	
	slope	intercept	$k_A(T_0)$ (mol/g·s)	E_A (kJ/mol)
$\ln k_A$ vs. $\left(\frac{1}{T} - \frac{1}{T_0}\right)$	-846.72	-17.53	2.42×10^{-8}	7.04
			$K_A(T_0)$ (mol/g·s)	ΔH_{ads} (kJ/mol)
$\ln K_A$ vs. $\left(\frac{1}{T} - \frac{1}{T_0}\right)$	2025.00	-3.28	3.75×10^{-2}	-16.83

Note: a. $k_A(T_0)$ or $K_A(T_0)$ is determined by taking the exponential of the corresponding intercept. E_A or ΔH_{ads} is determined by multiplication the corresponding negative slope with the gas constant

Table 5.12 Parameter estimates obtained from nonlinear regression analysis of a combined set of kinetic data obtained at three temperatures based on a first-order LHHW rate expression. The relative humidity is 0%.

parameter	Parameter estimation \pm 95% confidence interval
$k_{A,T0}$ (mol/g·s)	$1.92 \times 10^{-7} \pm 1.80 \times 10^{-7}$
$K_{A,T0}$ (Pa ⁻¹)	$1.64 \times 10^{-3} \pm 2.25 \times 10^{-3}$
E_A (J/mol)	$2.50 \times 10^4 \pm 8.40 \times 10^4$
ΔH_{ads} (J/mol)	$-1.13 \times 10^4 \pm 1.06 \times 10^5$

Table 5.13 Parameter estimates obtained from nonlinear regression analysis of a combined set of kinetic data obtained at three temperatures based on a first-order LHHW rate expression. The relative humidity is 100%.

parameter	Parameter estimation \pm 95% confidence interval
$k_{A,T0}$ (mol/g·s)	$2.42 \times 10^{-8} \pm 1.37 \times 10^{-9}$
$K_{A,T0}$ (Pa ⁻¹)	$3.75 \times 10^{-3} \pm 1.17 \times 10^{-3}$
E_A (J/mol)	$6.78 \times 10^3 \pm 2.85 \times 10^3$
ΔH_{ads} (J/mol)	$-1.58 \times 10^4 \pm 1.63 \times 10^4$

The activation energies of the reaction determined from the model were 25.02 and 6.78 kJ/mol at 0 and 100% relative humidity, respectively. The values of 25.02 and 6.78 kJ/mol for the activation energies of the reaction differed slightly from other researchers. Fu and coworkers (1996) reported that the apparent activation energies for photocatalytic oxidation of ethylene over the pure TiO₂ in water-free feed stream ([H₂O] < 5 ppmv) and relatively high water vapor content feed stream ([H₂O] = 1500 ppmv) were 13.9 and 16.0 kJ/mol, respectively. The activation energy of 14.2 kJ/mol was reported by Obee and Hay (1997) for the photocatalytic oxidation of ethylene over a glass slide coated with titania. Sirisuk (2003) also reported that the activation energy for photocatalytic oxidation of ethylene over borosilicate glass ring coated with titania was 7.5 kJ/mol and 13.04 kJ/mol, when the effect of the light irradiance from the light bulbs was included. From Tables 5.8 and 5.9, the reaction rate constants for 0% relative humidity were higher than those for 100% relative humidity at comparable temperatures despite the high activation energy. This observation may be attributed to difference in preexponential or frequency factor. The frequency factor involves a collision between reactant molecules. Therefore, in the presence of water, the frequency factor would be less than that with no water in the feed stream. The frequency factors of this reaction, as determined from the plot of $\ln k_A$ versus $1/T$, were 3.01×10^{-4} and 2.85×10^{-7} at 0% and 100% relative humidity, respectively.

The enthalpies of adsorption of ethylene in this reaction were -11.3 and -15.8 kJ/mol at 0 and 100% relative humidity, respectively. The negative sign indicated that the adsorption of ethylene on the surface was an exothermic process. The adsorption phenomena can be classified as physisorption and chemisorption (see Appendix D). The enthalpy change in this reaction suggested that the process was probably a weak form of chemisorption because the enthalpy change for physical adsorption is 4 kJ/mol, while the enthalpy change for chemisorption is 20-400 kJ/mol. The enthalpies of adsorption of ethylene at both relative humidity were similar to the values reported by other researchers. Fu and coworker (1996) reported that the enthalpy of adsorption of ethylene was in the range -13.4 to -15.9 kJ/mol while the value of -14.15 kJ/mol was reported by Sirisuk (2003) for the photocatalytic oxidation of ethylene over borosilicate glass ring coated with titania. Obee and Hay (1997) also reported that the

enthalpy of adsorption of ethylene over a glass slide coated with titania was 10.9 kJ/mol.



สถาบันวิทยบริการ
จุฬาลงกรณ์มหาวิทยาลัย

N CHAPTER VI

CONCLUSIONS AND RECOMMENDATIONS FOR FUTURE RESEARCH

This chapter summarizes experimental results involving characterization of titania and kinetic studies of the photocatalytic oxidation of ethylene. Recommendations for future research are also presented.

6.1 Conclusions

This research was divided into two parts. The first part involved the characterization. The second part involved kinetic studies.

6.1.1 Characterization of titania

Titania was prepared via a sol-gel method and calcined at 350 °C for 3 hours. Both anatase and rutile phase were found in the catalyst. The crystallite size of anatase of titania was approximately 5 nm while the crystallite size of rutile could not be determined because the observed rutile peaks were too small. . The specific surface area of titania was 134 m²·g⁻¹.

6.1.2 Kinetic studies of the photocatalytic oxidation of ethylene

This study investigated the effects of the concentration of water vapor in the feed and the reaction temperature on the photocatalytic oxidation of ethylene over titanium dioxide. A packed bed reactor was employed to determine the rates for the photooxidation of ethylene. Nonlinear regression analysis was employed to fit the kinetic data to a model. The kinetic data were best described by a LHHW rate expression. The best fit the data was Model 1 that represented a competitive adsorption between ethylene and water on active sites. Therefore, the photocatalytic oxidation rates of ethylene decreased with increasing concentration of water.

Activation energies for the photocatalytic oxidation of ethylene at 0 and 100% relative humidity were determined to be 25.02 and 6.78 kJ/mol, respectively. Enthalpies of adsorption of ethylene were -11.3 and -15.8 kJ/mol for 0 and 100% relative humidity, respectively. The adsorption of ethylene on the titania surface was an exothermic process. This process was a weak form of chemisorption

6.2 Recommendations for future research

1. The binary metal oxide should be further employed as a photocatalyst in order to compare activities with pure TiO_2 over photocatalytic oxidation of volatile organic compound.
2. Effect of water vapors at the different temperature should be further investigated so as to study how water vapors affect the activation energy and enthalpies of adsorption of ethylene.

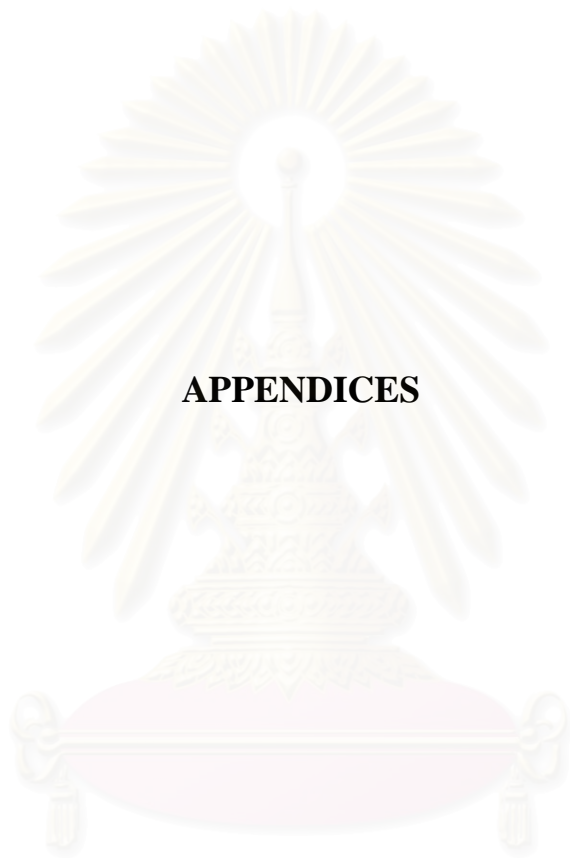
REFERENCES

- Alherici, R.M., and Jardim, W.F. Photocatalytic destruction of VOCs in the gas phase using titanium dioxide. Appl. Catal. B 14 (1997): 55-68.
- Amama, P. B., Itoh, K., Murabayaashi, M. Photocatalytic degradation of trichloroethylene in dry and humid atmospheres: role of gas-phase reactions. J. Mole. Catal. A: Chem. 217 (2004): 109-115.
- Anderson, M.A., Yamazaki-Nishida, S., and Carvera-March, S. Photodegradation, in D.F.Ollis and Al-Ekabi (eds.), Photocatalytic purification and treatment of water and air, Elsevier, Amsterdam, 1993, pp. 405-420.
- Bowker, M., Millard, L. Photocatalytic water-gas shift reaction at ambient temperature. J. Photochem. Photobiol. A: Chem. 148 (2002): 91-95.
- Cho, K., Hwang, K., Sano, T., Takeuchi, K., Matsuzawa, S. Photocatalytic performance of Pt-loaded TiO₂ in the decomposition of gaseous ozone. J. Photochem. Photobiol. A: Chem. 161 (2004): 155-161.
- Demeestere, K., Visscher, A. D., Dewulf, J., Leeuwen, M. V., Langenhole, H. V. A new kinetic model for titanium dioxide mediated heterogeneous photocatalytic degradation of trichloroethylene in gas-phase. Appl.Catal.B:Environ. 54(2004): 216-274.
- Devahasdin, S., Chiun, Jr. F., Li, K., Chen, D. H. TiO₂ photocatalytic oxidation of nitric oxide: transient behavior and reaction kinetics. J. Photochem. Photobiol. A: Chem. 156 (2003): 161-170.
- Falconer, J.L., Magrini-Bair. Photocatalytic and thermal catalytic oxidation of acetaldehyde on Pt/TiO₂. J. Catal. 179 (1998): 171-178.
- Fogler, H. S. Elements of Chemical Reaction Engineering, 3rd ed., Prentice-Hall, New Jersey., 1999.
- Fox, M. A., Dulay, M.T. Heterogeneous Photocatalysis. Chem.Rev. 93 (1993): 341-357.
- Fu, X., Clark, L. A., Zeltner, W. A., Anderson, M. A. Effect of reaction temperature and water vapor content on the heterogeneous photocatalytic oxidation of ethylene. J. Photochem. Photobiol. A: Chem. 97 (1996): 181-186.
- Gonzalez-Elipse, A. R., Munuera, G., Soria, J. Photo-adsorption and photodesorption of oxygen on highly hydroxylated TiO₂ surface, Part2-study of radical

- intermediate by electron paramagnetic resonance. J. Chem. Soc. Faraday Trans. I. 75 (1979): 748-756.
- Hager, S., Bauer, R., Kudielka, G. Photocatalytic oxidation of gaseous chlorinated organics over titanium oxide. Chemosphere. 41 (2000): 1219-1225.
- Hung, C., Marinas, B. J. Role of water in the photocatalytic degradation of trichloroethylene vapor on TiO₂ film. Environ. Sci. & Technol. 31 (1997): 1440-1445.
- Hennezel, D., Pichat, O. P., Oillis, D. F. Benzene and toluene gas-phase photocatalytic degradation over H₂O and HCl pretreated TiO₂: by-products and mechanisms. J. Photochem. Photobiol. A: Chem. 118 (1998): 197-204.
- Honmig, L., Zhiwei, L., Xiaojiang, Y., Wenfeng, S. Kinetic analysis of photocatalytic oxidation of gas-phase formaldehyde over titanium dioxide. Chemosphere. 60 (2005):630-635.
- Jacoby, W. A., Blake, D. M., Fennell, J.A., Boulter, J.E., Vargo, L. M., George, M. C., Dolberg, S. K. Heterogeneous photocatalysis for control of volatile organic compounds in indoor Air, J. Air & Waste Manage. Assoc. 46 (1996): 891-904.
- Kumar, S., Fedorov, A. G., Gole, J. L. Photodegradation of ethylene using visible light responsive surfaces prepared from titania nanoparticle slurries. Appl. Catal. B: Environ. 57 (2005): 93-107.
- Li, Y., White, T., and Lim, S. Structure control and its influence on photoactivity and phase transformation of TiO₂ nano-particles. Rev. Adv. Mater. Sci. 5 (2003): 211-215.
- Linsebigler, A. L., Lu, G. and Yates, Jr. J. T. Photocatalysis on TiO₂ surfaces: principles, mechanism, and selected results. Chem. Rev. 95 (1995): 735-758.
- Litter, M.L. Heterogeneous photocatalysis transition metal ions in photocatalytic systems. Appl. Catal. B: Environ. 23 (1999): 89-114.
- Meng, Y., Huang, X., Wu, Y., Wang, X., Qian, Y. Kinetic study and modeling on photocatalytic degradation of *para*-chlorobenzoate at different light intensities. Environ. Pollu. 117 (2002) 307-313.
- Obee, T. N., Brown, R. T. TiO₂ photocatalysis for indoor air application: effect of humidity and trace contaminant levels on the oxidation rates of formaldehyde, toluene, and 1,2-butadiene. Environ. Sci. & Technol. 29 (1995): 1223-1231.
- Obee, T. N., Hay, S. O. Effect of Moisture and Temperature on the Photooxidation of Ethylene on Titania. Environ. Sci. Technol. 31 (1997): 2034-2038.

- Park, D-R., Zhang, J., Ikeue, K., Yamashita, H., Anpo, M. Photocatalytic Oxidation of Ethylene to CO₂ and H₂O on Ultrafine Powdered TiO₂ Photocatalysts in the Presence of O₂ and H₂O. J. Catal. 185 (1999): 114-119.
- Peral, J., Ollis, D. F. Heterogeneous photocatalytic oxidation of gas-phase organics for air purification: acetone, 1-butanol, butylaldehyde, and m-xylene oxidation. J. Catal. 136 (1992): 554-565.
- Raillard, C., Hequet, V., Cloirec, P., Legrand, J. TiO₂ coating types influencing the role of water vapor on the photocatalytic oxidation of methyl ethyl ketone in the gas phase. Appl. Catal. B: Environ. 59 (2005): 213-220.
- Raillard, C., Hequet, V., Cloirec, P., Legrand, J. Kinetic study of ketone photocatalytic oxidation in gas phase using TiO₂-containing paper: effect of water vapor. J. Photochem. Photobiol. A: Chem. 163 (2004): 425-431.
- Raupp, G. B., Junio, C. T. Photocatalytic oxidation of oxygenated air toxics. Appl. Surf. Sci. 72 (1993): 321-327.
- Robertson, P. K. J. Semiconductor photocatalysis: an environmentally acceptable alternative production technique and effluent treatment process. J. Cleaner Prod. 4 (1996): 203-212.
- Saad, M. A. Thermodynamics Principles and Practice, Prentice-Hall, New Jersey., 1997.
- Sirisuk, A. Photocatalytic oxidation of ethylene over thin films of titanium dioxide supported on glass rings. Doctor of Philosophy, University of Wisconsin., 2003.
- Sirisuk, A., Hill, C., and Anderson, M. Photocatalytic degradation of ethylene over thin films of titania supported on glass rings. Catal. Today. 54 (1999): 159-164.
- Tawkaew, S. Preparation of semiconductor/layered compound nanocomposites and their photocatalytic activity for water pollution control. Doctor of Philosophy, University of Tohoku., 2002.
- Wan-kuen, J., Jung-Hoon, P., Hee-Dong, C. Photocatalytic destruction of VOCs for in-vehicle air cleaning. J. Photochem. Photobiol. A: Chem. 148 (2002): 109-119.
- Wang, K-H., Hsieh, Y-H. Heterogeneous photocatalytic degradation of trichloroethylene in vapor phase by titanium dioxide. Environ. Inter. 24 (1997): 267-274.

- Wang, K-H., Hsieh, Y-H., Lin, C-H., Chang, C-Y. The study of the photocatalytic degradation kinetics for dichloroethylene in vapor phase. Chemosphere. 39 (1999): 1371-1384.
- Wang, K-H., Tsai, H-H., Hsieh, Y-H. The kinetics of photocatalytic degradation of trichloroethylene in gas phase over TiO₂ supported on glass bead. Appl. Catal. B: Environ. 17 (1997): 313-320.
- Wu, J-F., Hung, C-H., Yuan, C-S. Kinetic modeling of promotion and inhibition of temperature on photocatalytic degradation of benzene vapor. J. Photochem. Photobiol. A: Chem. 170 (2005): 299-306.
- Yamazaki, S., Tanaka, S., Tsukamoto, H. Kinetic studies of oxidation of ethylene over a TiO₂ photocatalyst. J. Photochem. Photobiol. A: Chem. 121 (1999): 55-61.
- Yamazaki, S., Tsukamoto H., Araki, K., Tanimura, T., Tejedor-Tejedor, I., Anderson, M. A. Photocatalytic degradation of gaseous tetrachloroethylene on porous TiO₂ pellets. Appl. Catal. B: Environ. 33 (2001): 109-117.
- Zhang, P., Liu, J. Photocatalytic degradation of trace hexane in the gas phase with and without ozone addition: kinetic study. J. Photochem. Photobiol. A: Chem. 167 (2004): 87-94.
- Zhao, J., Yang, X. Photocatalytic oxidation for indoor air purification : a literature review. Build. Environ. 38 (2003):645-654.



APPENDICES

สถาบันวิทยบริการ
จุฬาลงกรณ์มหาวิทยาลัย

APPENDIX A

CALCULATION OF THE RATE CONSTANT AND THE ADSORPTION EQUILIBRIUM CONSTANT

The entering concentration of ethylene can be calculated from the entering temperature and pressure using the ideal gas law.

$$C_{A0} = \frac{P_{A0}}{RT_0} = \frac{y_{A0}P_0}{RT_0} \quad (\text{A.1})$$

where P_0 = entering total pressure = 2.39 atm

y_{A0} = entering mole fraction of ethylene = 0.001

T_0 = entering temperature = 32 °C = 305.13 K

R = ideal gas constant = 0.82 dm³·atm/mol·K

Substituting values in Equation A.1 yield

$$C_{A0} = \frac{0.001(2.39 \text{ atm})}{0.082 \frac{\text{dm}^3 \cdot \text{atm}}{\text{mol} \cdot \text{K}} \cdot (305.13 \text{ K})} = 9.55 \times 10^{-5} \frac{\text{mol}}{\text{dm}^3}$$
$$C_{A0} = 9.55 \times 10^{-5} \frac{\text{mol}}{\text{dm}^3} = 9.55 \times 10^{-5} \frac{\text{kmol}}{\text{m}^3} = 9.55 \times 10^{-8} \frac{\text{mol}}{\text{cc}}$$

The entering partial pressure of ethylene is

$$P_{A0} = y_{A0}P_0 \quad (\text{A.2})$$

$$P_{A0} = 0.001(2.39 \text{ atm}) = 2.39 \times 10^{-3} \text{ atm} = 239.2 \text{ Pa}$$

The entering molar flow rate of ethylene can be determined from the entering concentration, C_{A0} , and the entering flow rate, v_0 :

$$F_{A0} = C_{A0}v_0 \quad (\text{A.2})$$

The design equation for plug flow reactor is shown below:

$$\frac{W}{F_{A0}} = \frac{-1}{k_A K_A P_{A0}} \cdot \ln(1 - X_A) + \frac{1}{k_A} \cdot X_A \quad (\text{A.3})$$

where W = mass of catalyst = 0.4 g

X_A = fractional conversion of ethylene

k_A = rate constant

K_A = adsorption equilibrium constant of ethylene

The initial estimate for k_A and K_A can be obtained from linear regression analysis of the data in the form of a plot of $\frac{\ln(1 - X_A)}{X_A}$ versus $\frac{W}{F_{A0} \cdot X_A}$. The initial estimates of the parameters of LHHW models, k_A and K_A , can be calculated using the following equation.

$$k_A = -\frac{\text{slope}}{\text{intercept}} \quad (\text{A.4})$$

$$K_A = \frac{\text{intercept}}{P_{A0}} \quad (\text{A.5})$$

On the other hand, we can calculate k_A and K_A from the slope and intercept of a plot of $\frac{X_A}{\ln(1 - X_A)}$ versus $\frac{W}{F_{A0} \cdot \ln(1 - X_A)}$ using linear regression analysis. The initial estimate of the parameter can then be calculated using the follow equation.

$$k_A = \text{slope} \quad (\text{A.6})$$

$$K_A = \text{intercept} \cdot P_{A0} \quad (\text{A.7})$$

Example: Calculation of the rate constant and adsorption equilibrium constant to be used as using to be the initial estimate. The kinetic data obtained from the photocatalytic oxidation of ethylene at 90°C. The relative humidity is 100%.

Table A.1 Calculation of kinetic data in the form of $\frac{\ln(1 - X_A)}{X_A}$ and $\frac{W}{F_{A0} \cdot X_A}$. The reactions were performed at 90°C and 100% relative humidity.

No.	X_A	v_0 (cc/s)	F_{A0} (mol/s)(($\times 10^7$)	$\frac{W}{F_{A0}}$ (g.s/mol) ($\times 10^{-7}$)	$\ln(1 - x_A)$	$\frac{\ln(1 - X_A)}{X_A}$	$\frac{W}{F_{A0} \cdot X_A}$ (g.s/mol) ($\times 10^{-7}$)
1	0.0974	1.1710	1.1183	0.3577	-0.1024	-1.0521	3.6739
2	0.1378	0.7752	0.7403	0.5403	-0.1483	-1.0760	3.9209
3	0.3489	0.3018	0.2882	1.3878	-0.4291	-1.2298	3.9777
4	0.4472	0.2262	0.2161	1.8513	-0.5927	-1.3254	4.1402
5	0.6380	0.1433	0.1368	2.9236	-1.0160	-1.5926	4.5827
6	0.9509	0.0869	0.0830	4.8209	-3.0136	-3.1693	5.0699
7	0.9573	0.0775	0.0740	5.4031	-3.1543	-3.2949	5.6439
8	0.9583	0.0856	0.0818	4.8921	-3.1771	-3.3154	5.1051
9	0.9963	0.0673	0.0643	6.2241	-5.6112	-5.6318	6.2469

สถาบันวิทยบริการ
จุฬาลงกรณ์มหาวิทยาลัย

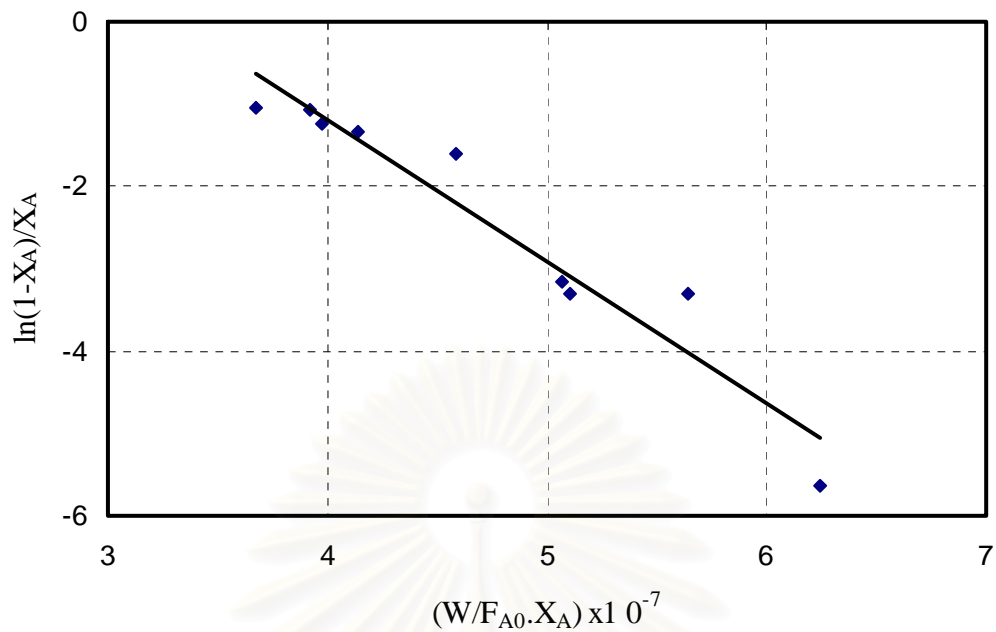


Figure A.1 The plot of data for photocatalytic oxidation of ethylene at 90°C based on Table A.1. The relative humidity is 100%.

สถาบันวิทยบริการ
จุฬาลงกรณ์มหาวิทยาลัย

Table A.2 Calculation of data in the form of $\frac{X_A}{\ln(1 - X_A)}$ and $\frac{W}{F_{A0} \cdot \ln(1 - X_A)}$. The reactions were performed at 90°C and 100% relative humidity.

No.	X_A	v_0 (ml/s)	F_{A0} (mol/s) ($\times 10^7$)	$\frac{W}{F_{A0}}$ (g.s/mol) ($\times 10^{-7}$)	$\ln(1 - x_A)$	$\frac{X_A}{\ln(1 - X_A)}$	$\frac{(W / F_{A0})}{\ln(1 - X_A)}$ (g.s/mol) ($\times 10^{-7}$)
1	0.0974	1.1710	1.1183	0.3577	-0.1024	-0.9505	-3.4920
2	0.1378	0.7752	0.7403	0.5403	-0.1483	-0.9294	-3.6441
3	0.3489	0.3018	0.2882	1.3878	-0.4291	-0.8131	-3.2343
4	0.4472	0.2262	0.2161	1.8513	-0.5927	-0.7545	-3.1236
5	0.6380	0.1433	0.1368	2.9236	-1.0160	-0.6279	-2.8776
6	0.9509	0.0869	0.0830	4.8209	-3.0136	-0.3155	-1.5997
7	0.9573	0.0775	0.0740	5.4031	-3.1543	-0.3035	-1.7129
8	0.9583	0.0856	0.0818	4.8921	-3.1771	-0.3016	-1.5398
9	0.9963	0.0673	0.0643	6.2241	-5.6112	-0.1776	-1.1092

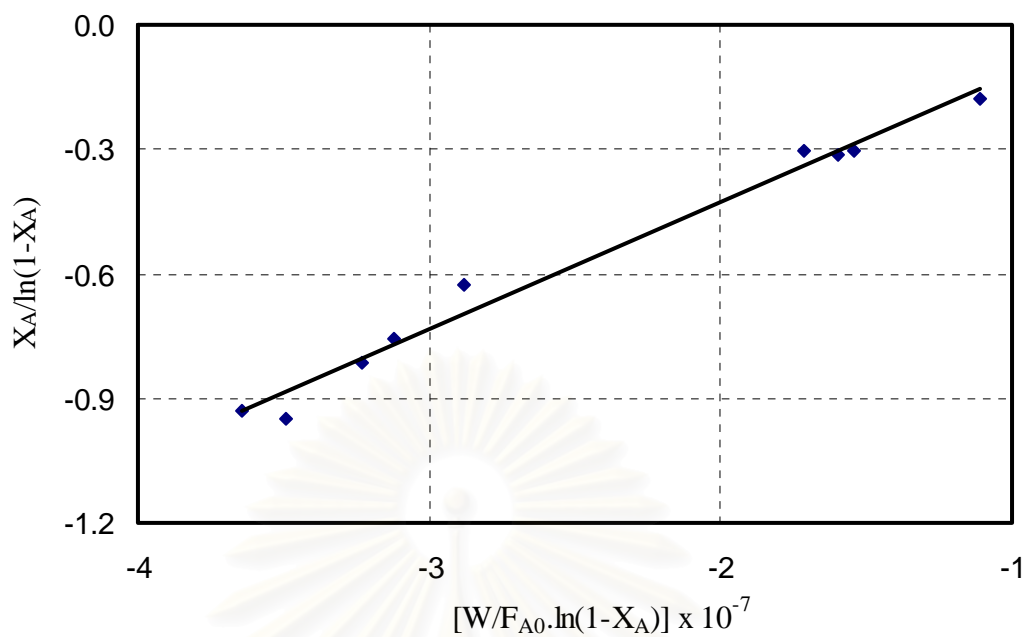


Figure A.2 The plot of data for photocatalytic oxidation of ethylene at 90°C based on Table A.2. The relative humidity is 100%.

สถาบันวิทยบริการ
จุฬาลงกรณ์มหาวิทยาลัย

Table A.3 Parameter estimates obtained from linear regression analyses of data for photocatalytic oxidation of ethylene at 90°C shown in Figures A.1 and A.2. The relative humidity is 100%.

Plot of	Linear regression parameters		Calculated parameters	
	slope	intercept	k_A (mol/g.s)	K_A (Pa ⁻¹)
$\frac{\ln(1 - X_A)}{X_A}$ vs. $\frac{W}{F_{A0} \cdot X_A}$	-2.0×10^{-7}	5.6665	3.53×10^{-8}	2.37×10^{-2}
$\frac{X_A}{\ln(1 - X_A)}$ vs. $\frac{W}{F_{A0} \cdot \ln(1 - X_A)}$	3.0×10^{-8}	0.1868	3.0×10^{-8}	44.69

สถาบันวิทยบริการ
จุฬาลงกรณ์มหาวิทยาลัย

APPENDIX B

CALCULATION OF THE VAPOR PRESSURE OF WATER

Calculation of vapor pressure of water by Antoine equation

From Antoine equation:

$$\log p = A - \frac{B}{T + C}$$

where p = the vapor pressure of water, mmHg.

T = the temperature in degree Celsius.

A , B , and C = Antoine constant

Example: The vapor pressure of water at 32°C is determined as follows;

$$\log p = 8.10765 - \frac{1750.286}{32 + 235} = 1.5523$$

$$p = 10^{1.5523} = 35.66 \text{ mmHg} = 4.755 \text{ kPa}$$

The vapor pressure of water at $32^{\circ}\text{C} = 4.755 \text{ kPa}$ and 20% relative humidity can be calculated:

$$\frac{20 \times 4.755}{100} \text{ kPa} = 0.955 \text{ kPa}$$

APPENDIX C

EXPRESSION OF THE RATE OF REACTION OF ETHYLENE

The overall reaction scheme of the oxidation of ethylene can be expressed as:



Langmuir-Hinshelwood-Hougen-Watson (LHHW) model was employed to discuss photocatalytic reactions. Several assumptions were made: (1) the heat of adsorption is the same for every molecule; (2) every molecule that strikes a molecule already adsorbed returns immediately to the gas phase; (3) oxygen and ethylene could be adsorbed on different site, and (4) the surface reaction is rate-limiting step. The various species in Equation 5.1 would be denoted: A = ethylene, O = Oxygen, C = Carbon dioxide, and W = Water. The reaction sequence for the decomposition is

The adsorption of ethylene on the surface:



The adsorption of oxygen on the surface:



The surface reaction to form adsorbed ethylene and oxygen in the gas phase:



The desorption of carbon dioxide and water from surface:



where S_I and S_{II} represent the active sites type *I* and *II*; respectively. $A \cdot S_I$, $C \cdot S_I$, $W \cdot S_I$, and $O \cdot S_{II}$ are the adsorption of ethylene, carbon dioxide, water on the sites S_I , and oxygen on the sites S_{II} ; respectively. k_1 , k_2 , and k_3 are the adsorption rate constant of ethylene, oxygen, and carbon dioxide and water; respectively. k_A is the reaction rate constant of ethylene. k_{-1} , k_{-2} , and k_{-3} are the desorption rate constant of ethylene, oxygen, and carbon dioxide and water; respectively.

The rate expression for the adsorption of ethylene as given in Equation C.1 is

$$r_1 = k_1 \cdot P_A \cdot C_{V_I} - k_{-1} \cdot C_{A \cdot S_I}$$

$$r_1 = k_1 \cdot \left(P_A \cdot C_{V_I} - \frac{C_{A \cdot S_I}}{K_A} \right) \quad (\text{C.5})$$

where K_A is the adsorption equilibrium constant for ethylene. C_{V_I} is the molar concentration of vacant sites type *I*. P_A is partial pressure of ethylene. $C_{A \cdot S_I}$ is surface concentration of sites type *I* occupied by ethylene. When the surface reaction is rate-limiting step, the adsorption rate constant of ethylene k_1 is large by comparison and we can set

$$\frac{r_1}{k_1} = 0 \quad (\text{C.6})$$

And solve Equation C.5 for $C_{A \cdot S_I}$:

$$K_1 = \frac{C_{A \cdot S_I}}{P_A \cdot C_V} \quad (\text{C.7})$$

The total concentration of sites type *I* is

$$C_{T_I} = C_{V_I} + C_{A.S_I} \quad (\text{C.8})$$

Rearranging gives Equation C.9

$$C_{V_I} = C_{T_I} - C_{A.S_I} \quad (\text{C.9})$$

Combining Equation C.7 and C.8 gives Equation C.9.

$$K_A = \frac{C_{A.S_I}}{P_A \cdot C_{V_I}} = \frac{C_{A.S_I}}{(C_{T_I} - C_{A.S_I}) \cdot P_A} = \frac{C_{A.S_I}}{C_{T_I} \cdot P_A - C_{A.S_I} \cdot P_A} \quad (\text{C.10})$$

Rearranging gives Equation C.11

$$C_{A.S_I} = \frac{K_A \cdot C_{T_I} \cdot P_A}{1 + K_A \cdot P_A} \quad (\text{C.11})$$

With a unit surface area and having $C_{A.S_I}$ defined as $\theta_{A,I}$, Equation C.11 becomes

$$\theta_{A,I} = \frac{K_A \cdot P_A}{1 + K_A \cdot P_A} \quad (\text{C.12})$$

In the similar manner, the surface concentration of adsorbed oxygen on sites type *II* (Equation C.2) can be written:

$$C_{O.S_{II}} = \theta_{O,II} = \frac{K_O \cdot P_O}{1 + K_O \cdot P_O} \quad (\text{C.13})$$

where K_O is the adsorption equilibrium constant for oxygen. P_O is partial pressure of oxygen. The rate of reaction, assuming that the surface reaction is the rate-limiting step, as given in Equation C.3 is

$$-r_A = k_A \cdot C_{A,S_I} \cdot C_{O,S_{II}} = k_A \cdot \theta_{A,I} \cdot \theta_{O,II} \quad (\text{C.14})$$

Substitution Equations C.12 and C.13 into Equation C.14 gives us

$$-r_A = \frac{k_A \cdot K_A \cdot P_A \cdot K_O \cdot P_O}{(1 + K_A \cdot P_A) \cdot (1 + K_O P_O)} \quad (\text{C.15})$$



สถาบันวิทยบริการ
จุฬาลงกรณ์มหาวิทยาลัย

APPENDIX D

CLASSIFICATION OF PHYSICAL AND CHEMICAL ADSORPTION

Adsorption Phenomena: Classification

Based on the nature of the bonding between the molecule and the surface, adsorption phenomena can be classified as physisorption and chemisorption. In physical adsorption, the only bonding forces are weak Van der Waals - type forces. There is no significant redistribution of electron density in either the molecule or at the substrate surface. In chemisorption, a chemical bond, involving substantial rearrangement of electron density, is formed between the adsorbate and substrate. The nature of this bond may lie anywhere between the extremes of virtually complete ionic or complete covalent character. The important classification between chemisorption and physisorption is shown in Table D.1.



สถาบันวิทยบริการ
จุฬาลงกรณ์มหาวิทยาลัย

Table D.1 Typical Characteristics of Adsorption Processes

Characteristics	Physical Adsorption	Chemical Adsorption
Binding force	Due to physical force of attraction, thus this process is also called as Van der waal's adsorption.	Due to chemical forces or bonding, thus this process is also called as activated adsorption.
Saturation uptake	Multilayer phenomena	Single layer phenomena
Activation energy	No activation energy involved.	May be involved.
Temperature range (over which adsorption occurs)	Adsorption is appreciable at lower temperature below boiling point of adsorbate	Adsorption can take place even at higher temperature.
Nature of sorbate	Amount of adsorbate removed depends more on adsorbate than on adsorbent.	Depends on both adsorbent and adsorbate.
Crystallographic specificity	Virtually independent of surface atomic geometry	Marked variation between crystal planes
Heat of adsorption	4 kJ/mol	20 - 400 kJ/mol

VITA

Miss Sureporn Sahnaphawuth was born on September 11, 1980 in Phitsanulok Province, Thailand. She received the Bachelor Degree of Chemical Engineering from Faculty of Engineering, Srinakharinvirot University in March 2004. In June 2004, she started her graduate study at department of Chemical Engineering, Chulalongkorn University.



สถาบันวิทยบริการ
จุฬาลงกรณ์มหาวิทยาลัย